NASA CONTRACTOR REPORT

NASA CR-1182

AN INVESTIGATION OF THIN FILM OXYGEN PARTIAL PRESSURE SENSORS

by T. M. Royal, J. J. Wortman, and L. K. Monteith

Prepared by
RESEARCH TRIANGLE INSTITUTE
Research Triangle Park, N. C.
for Langley Research Center

NATIONAL AERONAUTICS AND SPACE ADMINISTRATION • WASHINGTON, D. C. • SEPTEMBER 1968

NASA CR-1162

AN INVESTIGATION OF THIN FILM OXYGEN PARTIAL PRESSURE SENSORS

By T. M. Royal, J. J. Wortman,
and L. K. Monteith

Prepared under Contract No. NAS 1-7087 by
RESEARCH TRIANGLE INSTITUTE
Research Triangle Park, N.C.

for Langley Research Center

NATIONAL AERONAUTICS AND SPACE ADMINISTRATION

For sale by the Clearinghouse for Federal Scientific and Technical Information
Springfield, Virginia 22151 – CFSTI price $3.00

ABSTRACT

This study has been concerned with the design, development, and testing of a laboratory model of a thin film oxygen partial pressure sensor. Semiconducting zinc oxide and tin oxide films were investigated as the sensing element. Zinc oxide films at elevated temperatures were found to experience resistance changes greater than an order of magnitude when cycled from N_2 to O_2 environments. The zinc oxide films are relatively insensitive to other gases such as N_2, Ar, He, CO_2. A theoretical discussion of the physical mechanisms responsible for the observed phenomena is presented which is based on oxygen induced changes in the semiconductor donor and acceptor influences.

A suitable film substrate, heater, electrical contacting technique, and housing was designed and fabricated into a sensing head. The sensor head was coupled with a control unit for maintaining a constant operating temperature to form the complete sensor. Tests were performed to determine the operating characteristics of the unit.

CONTENTS

LIST OF ILLUSTRATIONS

LIST OF ILLUSTRATIONS (continued)

AN INVESTIGATION OF THIN FILM OXYGEN PARTIAL PRESSURE SENSORS

By T. M. Royal, J. J. Wortman,
and L. K. Monteith

SECTION I

INTRODUCTION

The objective of this research has been to determine the feasibility of using thin film devices as oxygen partial pressure sensors.

It has been known since the early 1900's that oxygen influences the electrical and optical properties of zinc oxide [Ref. 1]. Limited investigations performed under an earlier NASA study (NASA CR 66 306) showed that large reversible changes in the electrical conductivity of thin zinc oxide films were induced by changes in the oxygen partial pressure to which the films were exposed. In order to reach equilibrium in reasonable times following an environment change, it was necessary to heat the films. In the present study, the preparation of zinc oxide films and their electrical behavior in various environments have been studied.

Although much has been published on the electrical properties of zinc oxide single crystals and films, there are many contradictions and inconsistent results. This is because much of the work predates both the availability of pure materials and adequate measurement techniques. One consistent observation is that the history of exposure of a sample to oxygen has an important effect on the electrical and photo-properties of the material.

In this study, oxide films have been prepared by oxidizing zinc films at elevated temperatures. Their electrical conductivity has been measured as a function of temperature, oxygen partial pressure and other atmospheric constituents. The time response following partial pressure changes has also been investigated as a function of temperature and environmental changes.

Experimental investigations have also been made on tin oxide films to determine their potential usefulness as oxygen partial pressure sensors. It appears that zinc doped tin oxide is sensitive to oxygen partial pressure. However, the films are difficult to prepare in a consistent manner.

A detailed search of the literature has been made as a part of a theoretical study. Based on previous works and the present experimental observations, a theoretical treatment of the phenomena is presented. The

model is based on oxygen induced changes in the donor and acceptor contributions to the electrical conductivity of the semiconducting films. Although the mechanisms involved are complex and difficult to describe analytically, the model is consistent with experimental observations.

Much effort has been directed toward designing and fabricating a laboratory sensor. This has required the development of techniques for depositing the films, heating the films, providing reliable electrical contacts, and for constant temperature control.

Extensive tests on a laboratory model of the sensor have been performed in order to determine its operating characteristics. These tests indicate, with the one disadvantage of a long time constant, zinc oxide thin film partial pressure sensors appear very promising. Some of the attractive features are its simplicity, potential small size, low power, and large dynamic range.

SECTION II

SEMICONDUCTING FILMS

Experimental

Zinc oxide films were prepared by oxidizing zinc films in oxygen at elevated temperatures. The zinc films were prepared using standard vacuum evaporation techniques. Three different types of substrates were used for supporting the thin films of zinc. The first types were very thin Pyrex squares 2.2 cm on each side. Zinc exhibited very good adherence to Pyrex but these substrates limited the oxidation temperature to less than 550°C, the softening temperature of Pyrex glass. At this temperature it is difficult to completely oxidize the zinc film.

The second substrate material investigated was quartz, also in the form of 2.2 cm squares. These substrates allowed higher oxidizing temperatures, however, even with slow cooling, severe peeling and cracking destroyed the films. This was due to the thermal mismatch of the two materials.

The third experimental substrate was 96% pure alumina sheet approximately 2.0 cm square and 0.1 cm thick. The alumina substrate proved to be compatible with the zinc oxide thin films for all processes used in fabricating the oxygen sensor. Zinc oxide had excellent adherence characteristics on the alumina squares. The surface was slightly rougher than either Pyrex or quartz.

For electrical contacts to the zinc oxide, two types of metallizations were investigated. The first was a fired-on contact using liquid bright gold across each end of the substrate. At the elevated temperatures, the gold contacts degraded in a few days. When liquid bright platinum was substituted for the gold and the contacts were fired-on the substrate prior to evaporating the zinc, excellent electrical contacts were obtained. These did not degrade like the gold contacts. The liquid bright platinum area is fired at 450°C in air and cooled at approximately 100°C per hour.

The alumina substrates were ultrasonically cleaned with detergent, water, and alcohol before being placed in the vacuum system for the zinc evaporation. The zinc films were prepared in thicknesses ranging from 500 to 1000 Å with a vacuum of at least 10^{-4} torr. Films thicker than 1000 Å were also prepared and evaluated. These thicker films were very difficult to oxidize and also showed very long response times and decreased sensitivity. The condensation rate of the zinc on the substrate was found to be very dependent upon temperature and previous surface treatments of the substrate. For example, one surface treatment which was used requires precoating the substrate with a thin (< 100 Å) silver layer to enhance uniform condensation of the zinc [Ref. 2]. Cooling the substrate also helps in obtaining uniform film thickness. A few evaporations were performed

successfully without precoating with silver, however, most samples showed regions of nonuniform thickness for both cooled and uncooled samples.

The substrates were masked for evaporation by attaching glass slides to the substrate. In order to cool the substrate, it was attached to a cold plate of large thermal mass which was cooled with liquid nitrogen. The films were prepared using 99.99% purity zinc evaporated from a ceramic crucible heated with a helical-wound tungsten filament or directly from a tungsten boat. The particular source had no effect on film quality.

In preparing thin films of zinc, the diffusion of zinc vapor creates additional problems that do not occur when evaporating lower vapor pressure metals such as aluminum, silver, tin, gold, and nickel. Electrical feedthrough insulators in the vacuum chamber are plated and require cleaning after every evaporation. Zinc seems to coat almost everything in the vacuum chamber except the substrate. Even the use of a directional source such as a ceramic crucible with a restriction at the vapor exit did not prevent shorting of electrical connections in the system thus negating the use of a crystal mass monitor to measure the film thickness.

After evaporation the samples were placed in an oxygen atmosphere in a tube furnace at a temperature of approximately 27°C. The temperature was increased at a rate not exceeding 300°C per hour to a maximum of 600°C where it was held for a period of 4 to 8 hours. A four-hour oxidation period was generally sufficient to oxidize films of a thickness less than 1000 Å. The films were considered to be completely oxidized when the oxide film appeared to be translucent or transparent depending upon the initial thickness of the film.

The films were evaluated in a tube furnace. The total gas pressure in the tube was maintained at one atmosphere with different partial pressures obtained by mixing. The gas percentages were determined with ordinary glass flow meters (5% accuracy). Flow rates were kept low so that cooling effects on the films were reduced. Electrical connections were made to the platinum film contacts by gold pressure contacts.

Two types of electrical measurements were made on zinc oxide films: (1) electrical conductance, and (2) photoconductance. The electrical conductance (dark current) was found to vary over several orders of magnitude depending on temperature, time, and gas environment. The results obtained from the measurement of conductance as a function of temperature for the various environments can be divided in general into two categories: (1) transitory (seconds to minutes), and (2) equilibrium (minutes to hours). The equilibrium conditions will be discussed first.

Equilibrium Conditions. - Figure 1 shows a typical plot of log conductance as a function of reciprocal temperature for various oxygen partial pressures. When temperature is increased from room temperature with the films in oxygen, the conductivity first increases to a maximum then decreases, and then increases again for higher temperatures. The maximum occurs at approximately 500°K and the minimum at 650°K. As shown in Fig. 1,

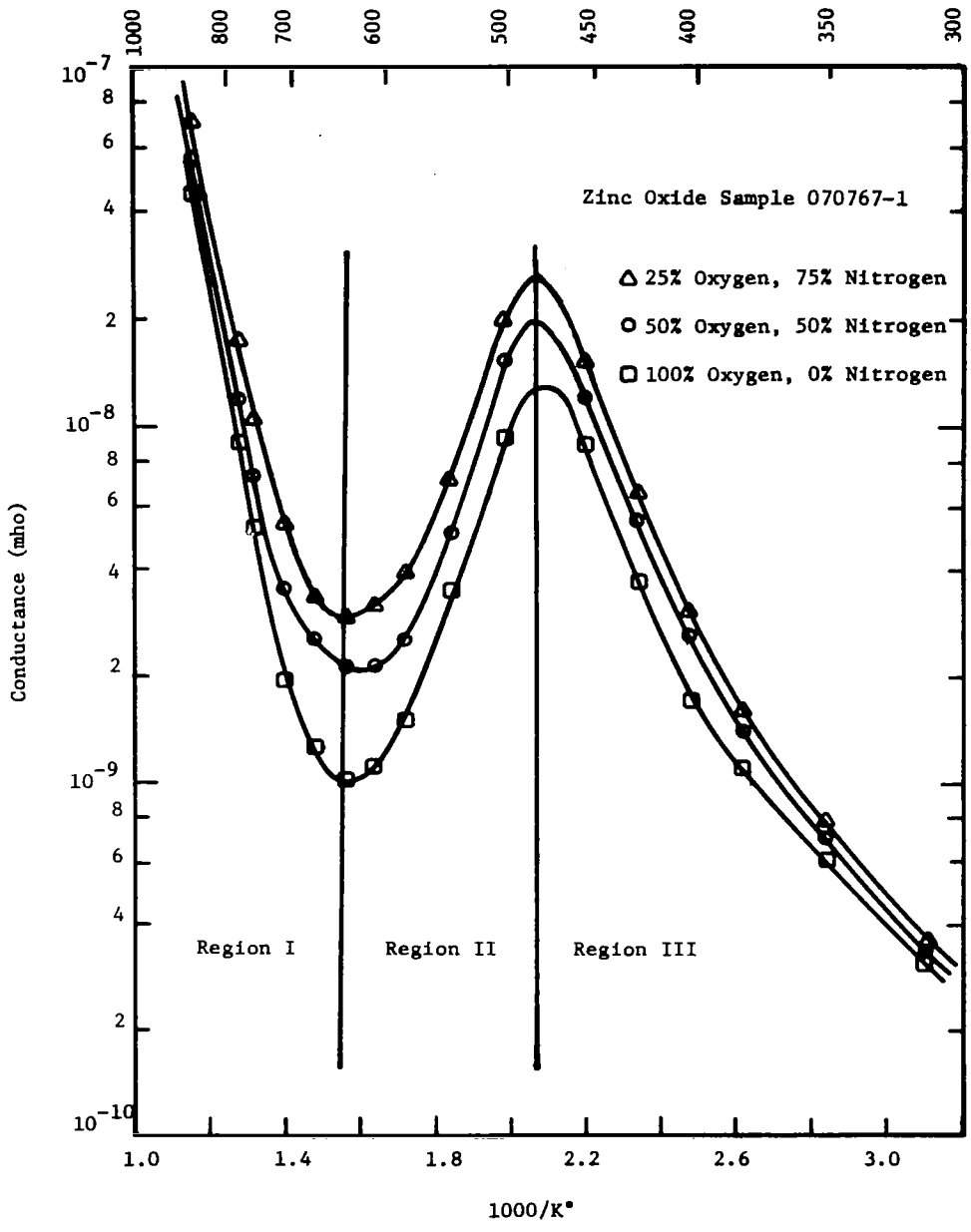

Figure 1. Electrical Conductance of Zinc Oxide vs. Increasing Temperature for Various Partial Pressures of Oxygen

at a constant temperature the film conductance is a strong function of the oxygen partial pressure. For example, at 700°K a change from 25% O_2 - 75% N_2 mixture to 100% O_2 - 0% N_2 results in a factor of three decrease in the film conductance. As also can be seen from Fig. 1, the conductivity dependence on oxygen partial pressure is temperature dependent.

The variation of the conductivity with oxygen partial pressure is shown on a semi-log graph in Fig. 2. Two different samples are shown in the figure and as can be seen the slopes are the same for the temperatures shown. The conductivity differs for the two samples by an order of magnitude and is a result of the film thickness. The thinner the film, the less the conductance. Efforts were made to determine the effect of film thickness on the phenomena. Attempts to make several films of various thicknesses on a single substrate for testing were not successful due to the difficulties of making consistent zinc films. By evaluating films made on different substrates and tested at different times such as those of Fig. 2, it was possible to draw some conclusions. As already stated, the slopes of conductance as a function of temperature are parallel for various film thicknesses and conductances. The major effect of film thickness appears to be a reduced time response with increased film thickness. For a sensor application the thinner the film the better the response time. This is a very difficult parameter to control using the present film preparation technique. Reactive sputtering may be a superior way to control film thickness.

Shown in Fig. 3 is the effect of slowly heating and cooling in N_2 on a film that was previously annealed in oxygen and allowed to cool slowly in the oxygen environment. Note the large separation between the heating and cooling curves at low temperature. The change in slope of the curves below the maximum deviates in the case of N_2 (zero O_2) from that exhibited by O_2 pressures as is seen in Fig. 1.

The data presented in Figs. 1 and 3 were obtained from measurements in which the sample was allowed to reach equilibrium following any temperature change. At the low temperatures the equilibrium time was very long (days). Also, the temperature was increased and decreased in small steps and the sample was allowed to reach equilibrium at each temperature (data point). The variation of conductance as a function of time for a typical sample is shown in Fig. 4 for one atmosphere of Ar, O_2, N_2, and He in turn. The response time is different for each gas.

Figures 5 and 6 are plots of conductance as a function of log time for a sample cycled from N_2 to O_2 and from O_2 to N_2. The response times are much longer for a decrease in oxygen partial pressure than they are for an increase. Figure 7 shows the response for a change from O_2 to CO_2, Ar, and He. Note that at long times the slopes are the same while at short times they differ. Typical response times for changing from one atmosphere of N_2 to one atmosphere of O_2 are approximately 70 seconds to reach 63% of the final value, while a change from O_2 to N_2 is approximately 10^3 seconds.

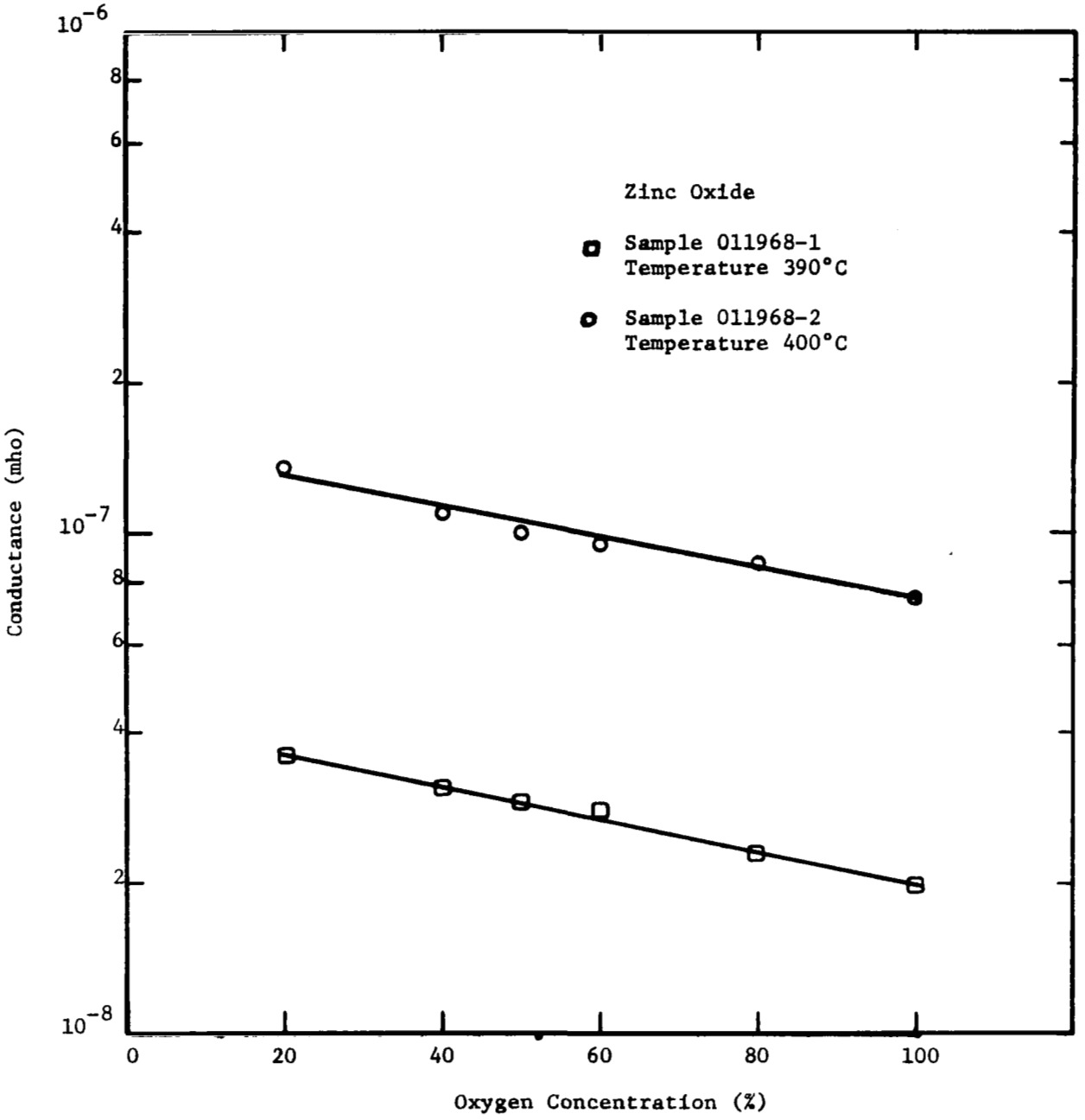

Figure 2. Electrical Conductance of Two Samples as a Function of Oxygen Partial Pressure

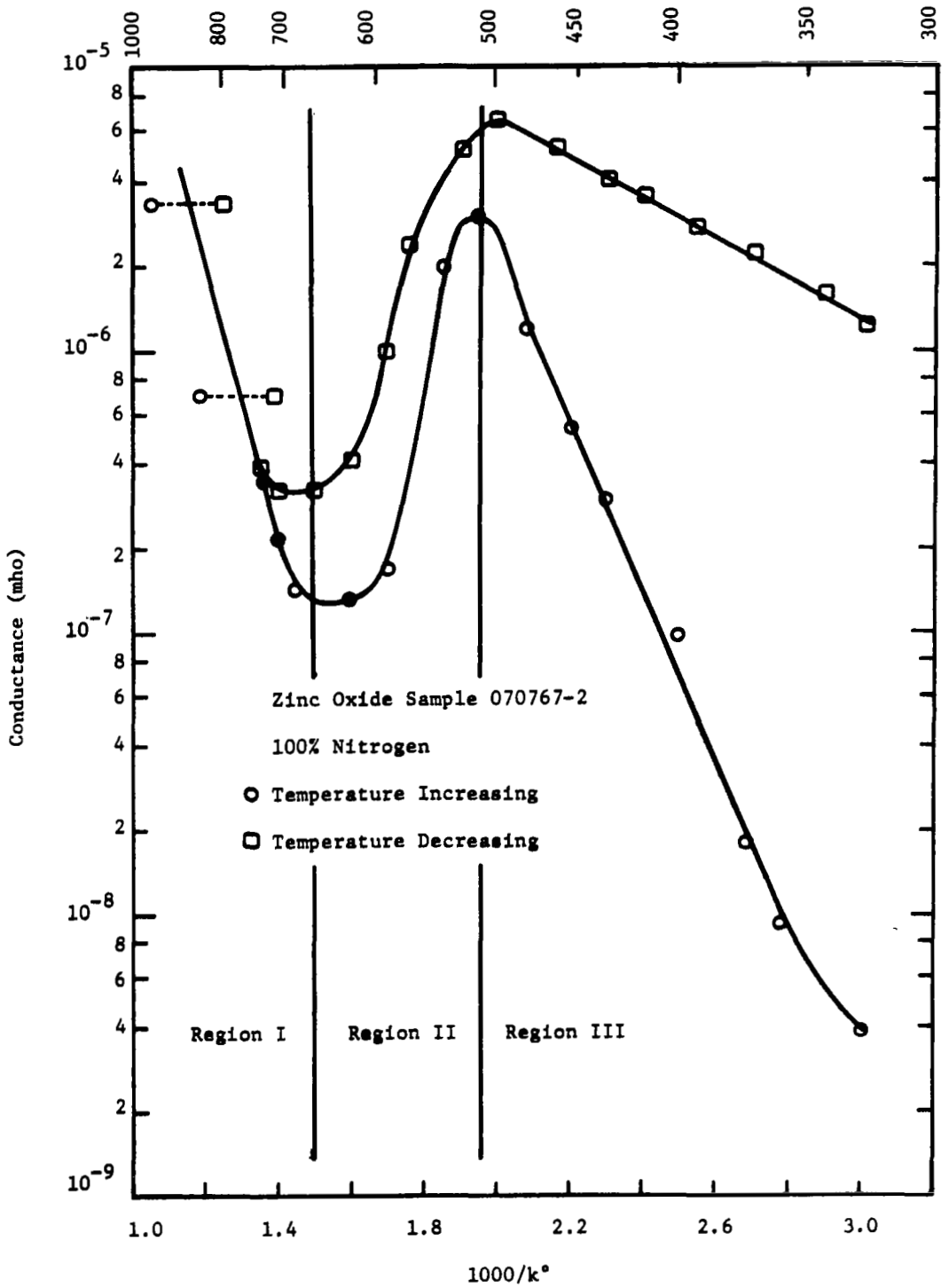

Figure 3. Electrical Conductance vs. Increasing and Decreasing Temperature

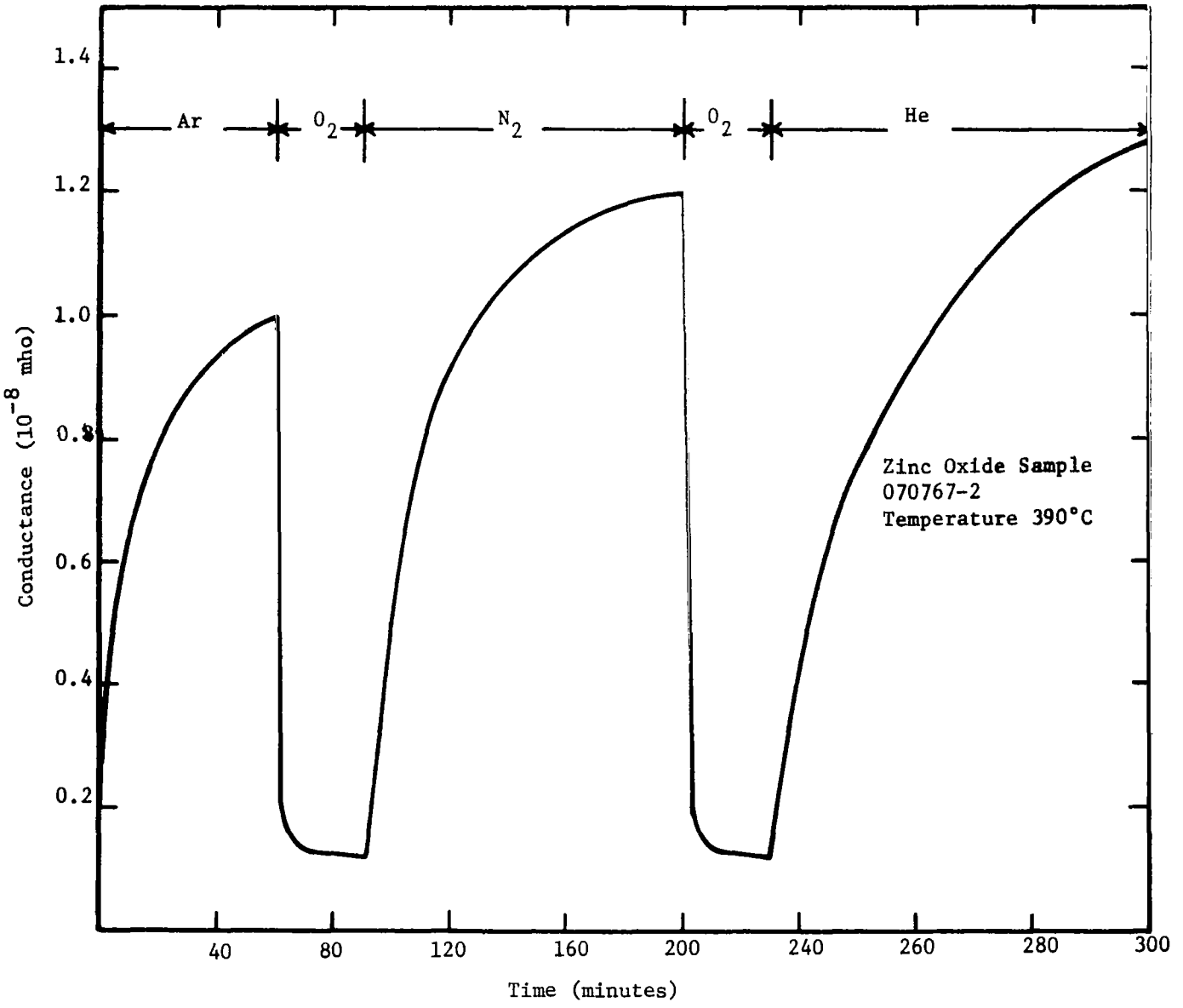

Figure 4. Response Time for Various Gases

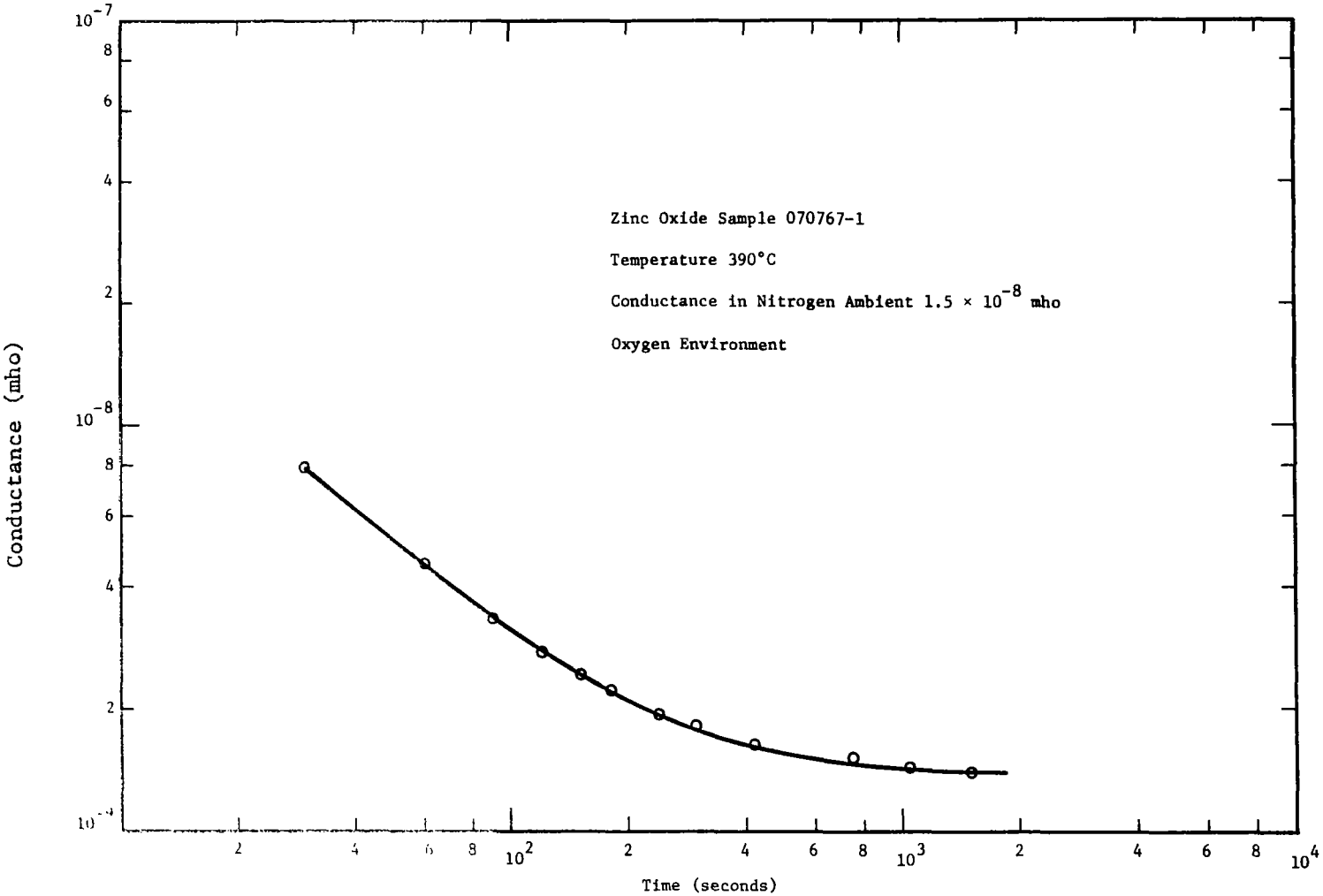

Figure 5. Electrical Conductance for an Environment Change from Nitrogen to Oxygen

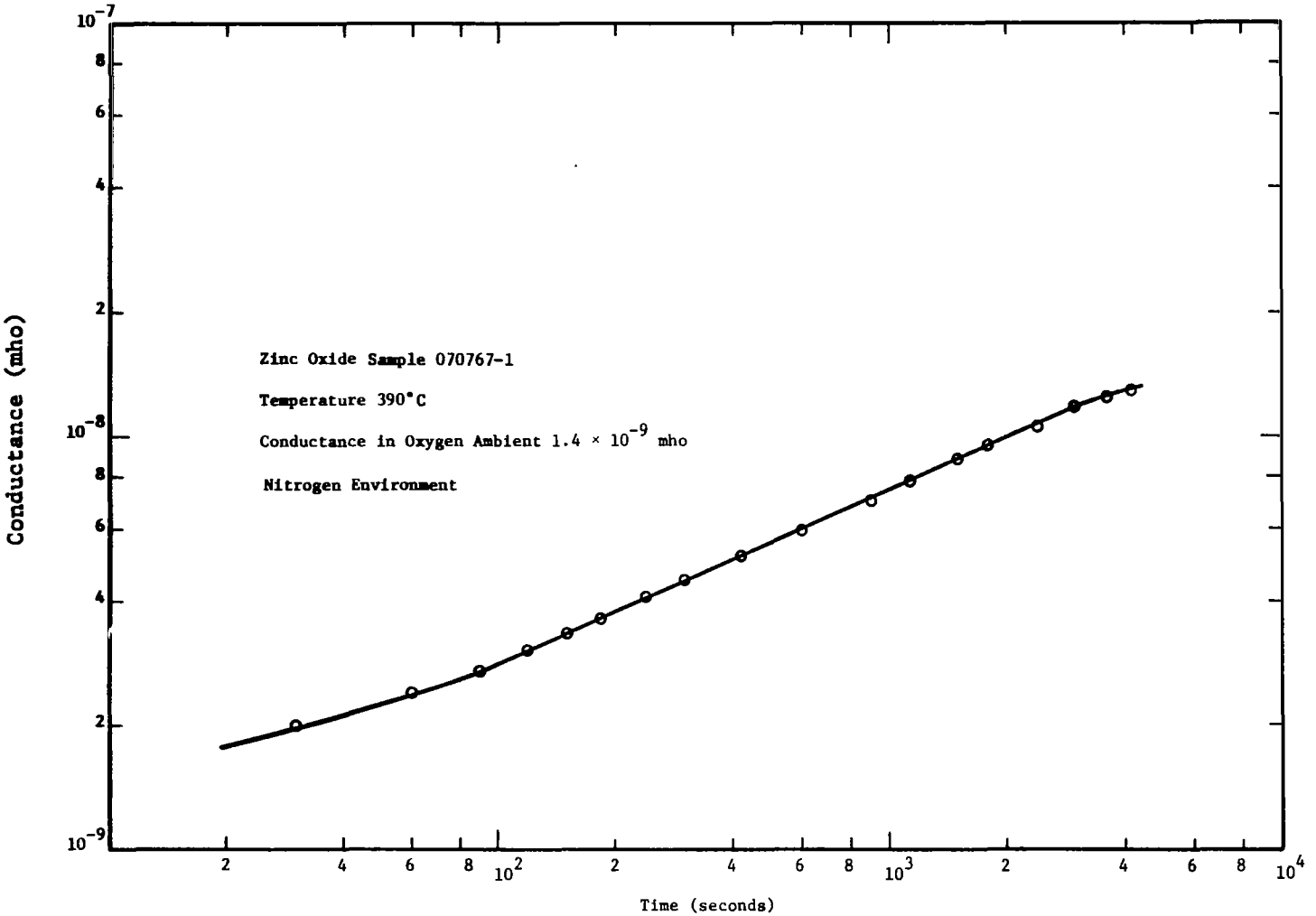

Figure 6. Electrical Conductance for an Environment Change from Oxygen to Nitrogen

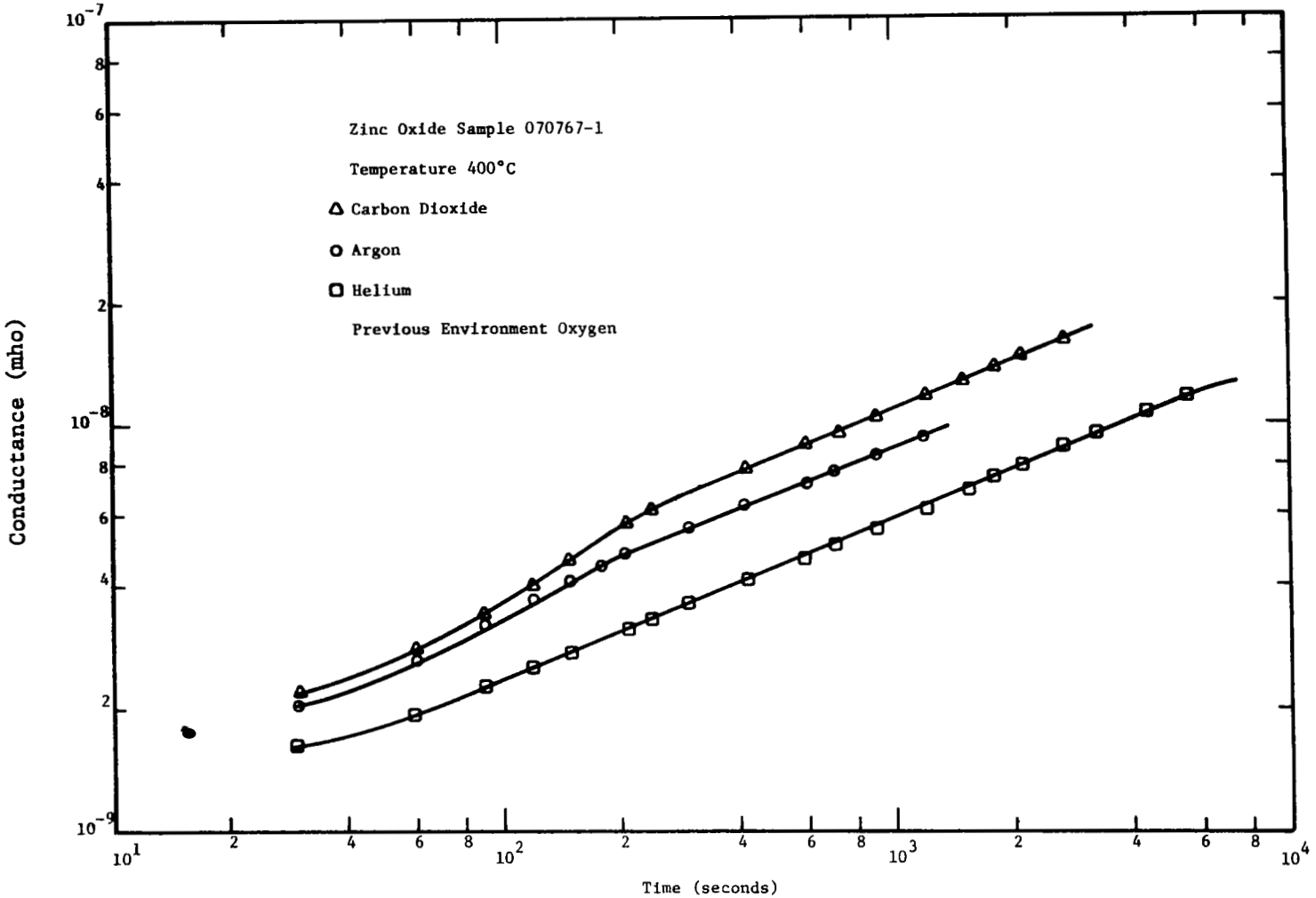

Figure 7. Transient Electrical Conductance for an Environment Change from Oxygen to Inert Gases

Transient Effects. - In the preceding discussion, the equilibrium effects were discussed. The conductivity dependence on temperature for the various environments is a function of time. As one might expect, if the conductivity is not allowed to stabilize following a temperature change, the temperature dependence is drastically altered.

Figure 8 is a plot of conductivity as a function of reciprocal temperature for various temperatures, 0_2 and N_2 environments, and rate conditions. The action starts on the lower curve at $10^3/T = 1.5$ in an 0_2 environment (curve 1). Temperature is decreased in two minute intervals with a total time lapse of approximately 1 hour to reach the low temperature. A 1 hour lapse with a 20 minute N_2 treatment resulted in the interim between curve 1 and curve 3. Curve 3 represents an increasing temperature in 0_2 with 2 minute intervals and approximately 1 hour to reach the high temperature end. Following curve 3, the environment was switched to N_2 and allowed to stabilize for 15 hours. Curve 5 represents a decreasing temperature in N_2 with 30 minute intervals with a total of approximately 8 hours. At the low end of curve 5 the sample remained in N_2 for 16 hours to reach the top of curve 7. Curve 7 represents another decrease at 30 minute intervals. Curve 9 immediately followed curve 7 and represents an increasing temperature at 2 minute intervals. At the top of curve 9 a 1 hour and 30 minute time elapsed. Curve 11 represents a decreasing temperature at 2 minute intervals.

The data presented in Fig. 8 shows the wide variety of conditions possible if equilibrium is not allowed to occur between changes. Several factors are important in the data of Fig. 8. For example, it is rather odd that most of the slopes are approximately the same with the exception of the high temperature curves of 5 and 9. Also note the lack of a minimum and maximum in curves 1, 3, and 11. The minimum and maximum occurred only during a rather slow run and immediately following the slow run in which the temperature was started from the low end. All fast runs which starting from the high temperature end resulted in no inflection points.

Photoconductivity Measurements. - In addition to testing the zinc oxide films at elevated temperatures by observing the electrical conductivity as a function of oxygen partial pressure, photoconductivity measurements were performed on zinc oxide films. The photoconductivity was measured using a xenon lamp with a flash rate of approximately ten flashes per second. The sample holder and circuit shown in Fig. 9 was used to monitor the photocurrent while the film was exposed to various gas environments at an absolute pressure of 1 atmosphere. Care was taken to prevent illumination of the contact region from xenon source. The illuminated area on the zinc oxide was approximately 0.5 cm^2. The duration of the xenon flash was approximately three microseconds. Typical oscilloscope traces of the photocurrent are shown in Figs. 10 and 11 for nitrogen and oxygen ambients at 27°C. Resistance changes of approximately 15% were observed between 100% nitrogen and oxygen environments.

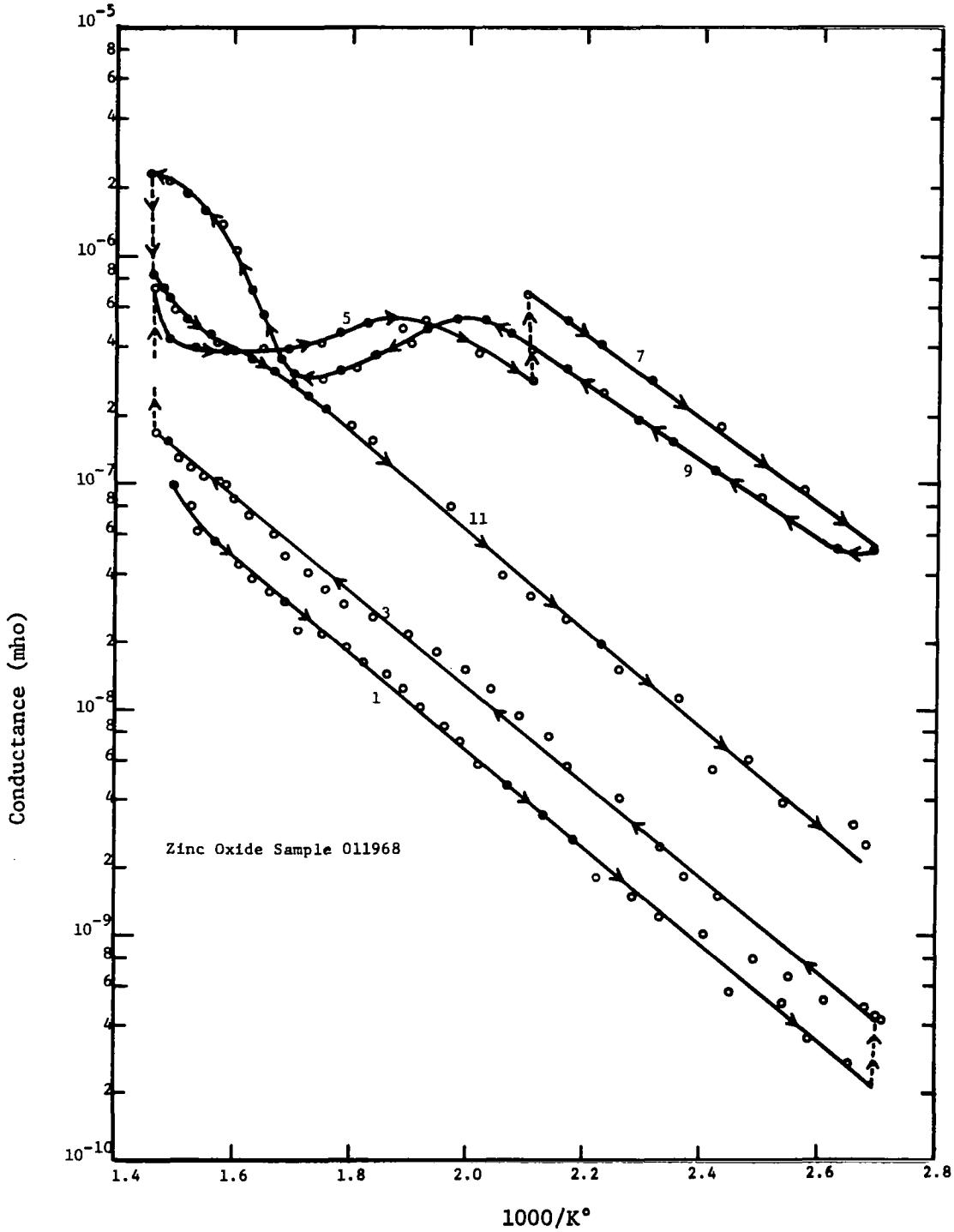

Figure 8. Conductance vs. Temperature as a Function of Various Heating and Cooling Rates

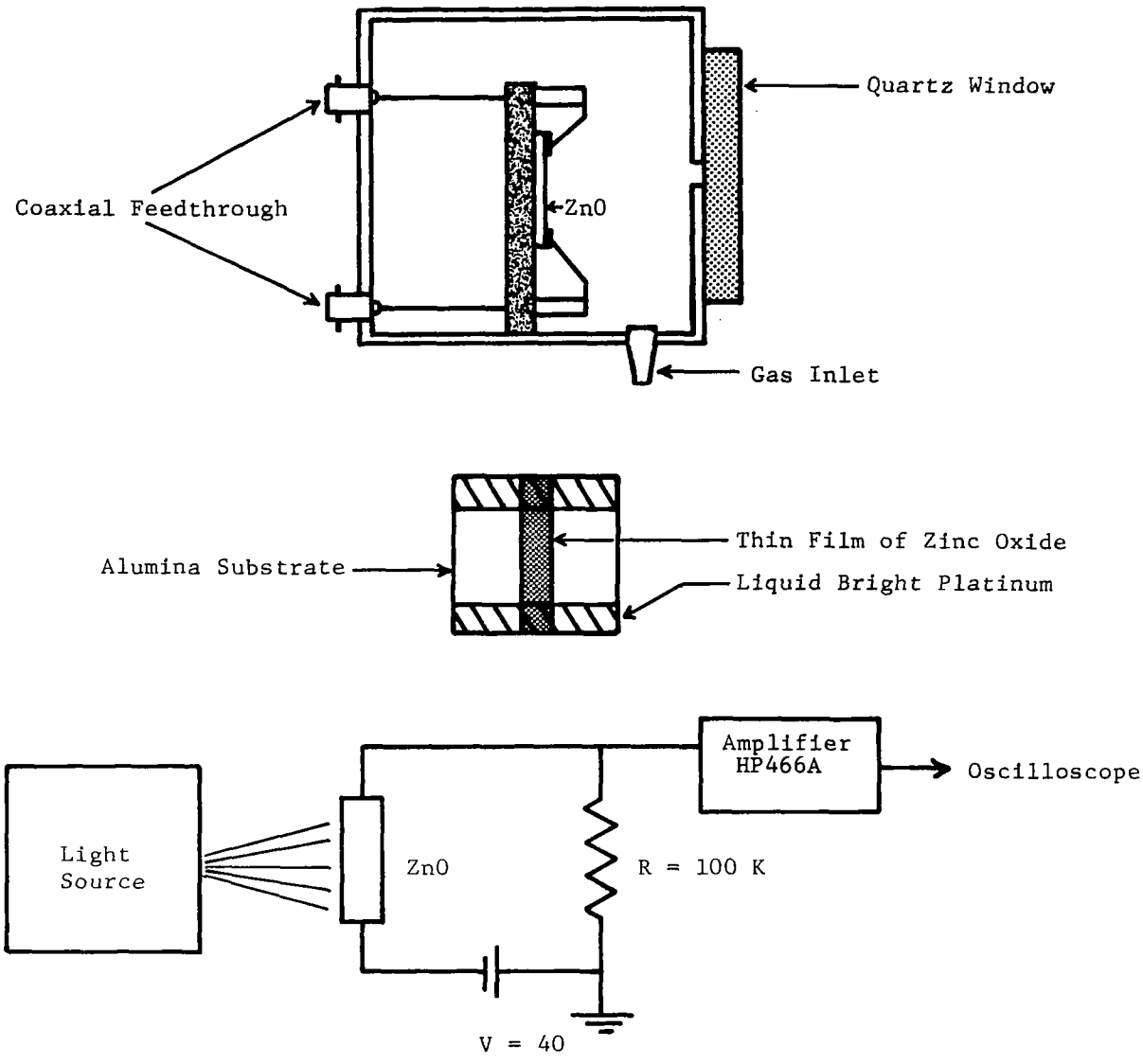

Figure 9. Photoconductivity Sample Holder and Circuit Arrangement for Measuring Photoresponse of Zinc Oxide in Nitrogen and Oxygen Environments

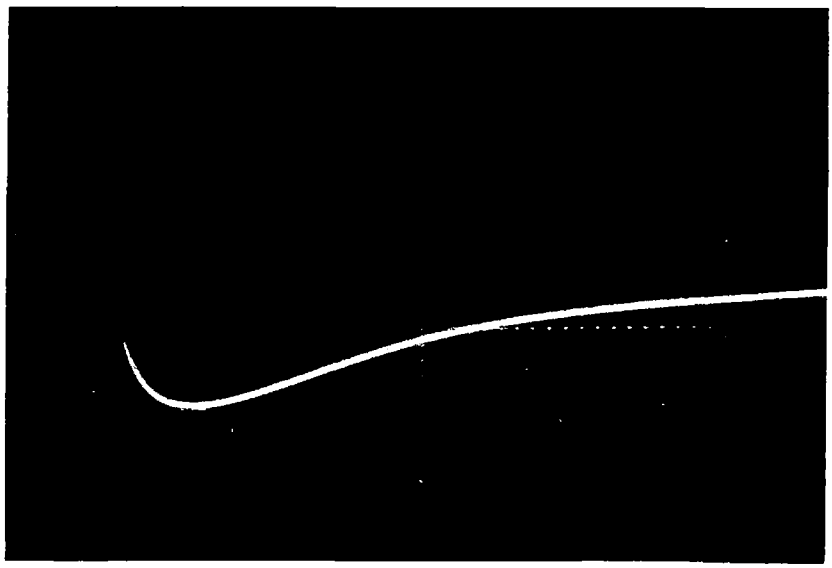

Figure 10. Typical Photoconductivity Response of Zinc Oxide Exposed to an Oxygen Environment. Horizontal - 20 μsec/div., Vertical - 0.2 μamp/div., Base Line - 0.5 div. from Top Grid Line.

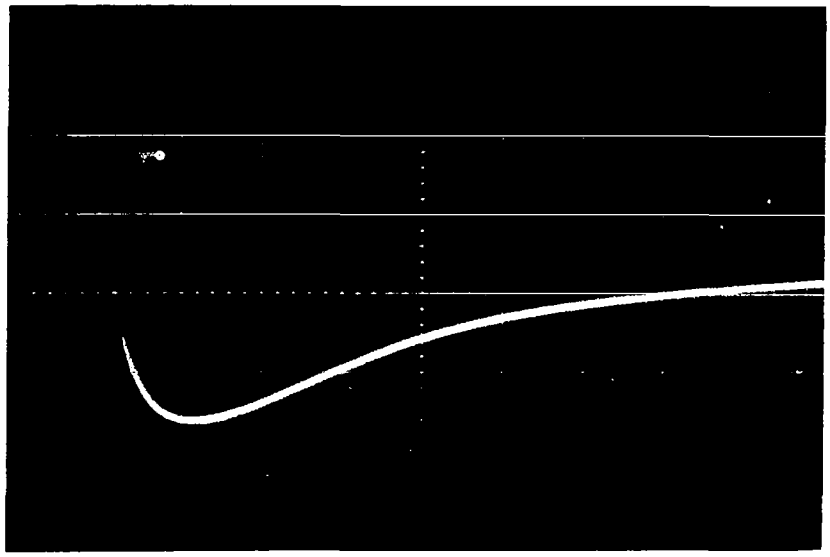

Figure 11. Typical Photoconductivity Response of Zinc Oxide Exposed to a Nitrogen Environment. Horizontal - 20 μsec/div., Vertical - 0.2 μamp/div., Base Line - 0.5 div. from Top Grid Line.

Two significant advantages of observing the photoconductivity at room temperature rather than the electrical conductivity at an elevated temperature is the elimination of the power required for the heater and the necessity of providing reliable high temperature electrical contacts to the sensing film. Further advantages, perhaps a shorter response time, may be possible by utilization of the photoresponse of zinc oxide.

Tin Oxide. - Thin films of tin were prepared using Pyrex substrates with liquid bright platinum contacts. After vacuum evaporating the tin films in the same system used for zinc, the films were oxidized in a tube furnace at approximately 300°C for about 8 hours. The electrical conductance of the tin oxide films when exposed to oxygen and nitrogen is shown in Fig. 12. To produce better tin oxide films, later evaporations were made in a vacuum system that was free of zinc contamination. The purer tin oxide films were much less sensitive than the films contaminated with zinc. Attempts to make zinc doped tin films reproducible were unsuccessful.

Photoconductivity measurements by Matthews [Ref. 3] indicate a photodecay with a dependence upon oxygen partial pressure for samples of tin oxide and tin oxide doped with zinc. The tin oxide films with small amounts of zinc possessed much shorter response times than those of pure zinc. The doped film was measured at 270°C while zinc oxide films are normally tested at 400°C. The stability of the tin oxide films doped with zinc was very poor compared to zinc oxide films.

Theoretical Discussion

As illustrated by the data in the preceding sections, the phenomena involved in the zinc oxide films are complex. In particular, the maximum followed by the minimum in the conductivity-temperature data and its dependence on oxygen pressure eliminates any simple explanation of the results. Numerous attempts have been made to understand the underlying physical mechanisms responsible for this behavior. A thorough review is given by Heiland, Mollwo and Stöckmann [Ref. 1]. Many of our observations have been observed by other workers in both single crystals and thin films. No attempt is made here to review all of this prior work, instead a physical model for the phenomena is proposed and compared to other models where appropriate.

General Model. - The semiconducting properties of zinc oxide give it the special properties observed experimentally. It may be described with equal validity either in semiconductor terminology or with chemical models. It is most appropriate here to discuss it in terms of the laws of mass action since only oxygen and zinc are involved in the system.

Zinc oxide (ZnO) crystallizes as an ionic crystal in the hexagonal wurtzite lattice in which the oxygen ions are in the hexagonal closest packed arrangement. Being a semiconductor means that any imperfections, defects, impurities or lack of stoichiometry in the system results in

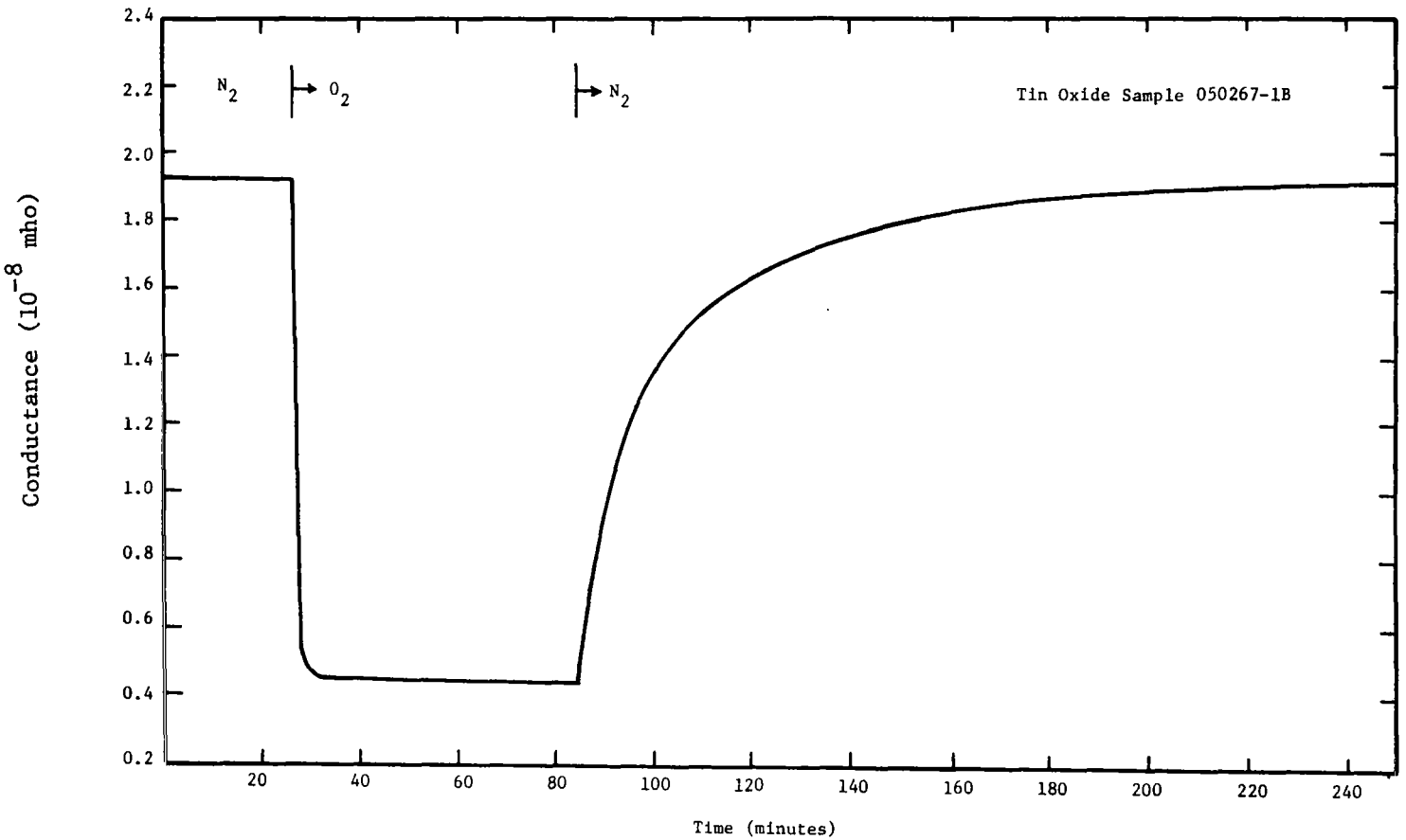

Figure 12. The Conductivity of Tin Oxide Doped with Zinc for Oxygen and Nitrogen Environments

important changes in the electrical properties. Only the excess or deficiency of zinc and oxygen need be considered here. These stoichiometric defects exist as interstitials, substitutionals, or vacancies in the crystalline lattice.

As interstitials, zinc atoms can behave as donors, i.e., ionize and give up electrons to the lattice. Oxygen on the other hand, in interstitial form, behaves as an acceptor, i.e., it ties up an electron. Their reactions may be expressed as:

$$Zn_i^{\times} \rightleftarrows Zn_i^{+} + e^{-} , \tag{1}$$

$$Zn_i^{\times} \rightleftarrows Zn_i^{++} + 2e^{-} , \tag{2}$$

and

$$O_i^{\times} \rightleftarrows O_i^{-} + e^{+} , \tag{3}$$

$$O_i^{\times} \rightleftarrows O_i^{--} + 2e^{+} , \tag{4}$$

where $Zn_i^{\times}$, $O_i^{\times}$ are neutral interstitial atoms and Zn_i^{+}, Zn_i^{++}, O_i^{-}, O_i^{--} are ions, e^{-} is an electron, and e^{+} is a hole, the $\times$ indicates neutral.

The role of substitutional defects is neglected here since both types would require the existence of special valence states. These are improbable. The third type of possible defect is the vacancy. Zinc and oxygen vacancies are not likely to occur simultaneously. An anion vacancy acts as a donor:

$$O_v^{\times} \rightleftarrows O_v^{+} + e^{-} , \tag{5}$$

$$O_v^{\times} \rightleftarrows O_v^{++} + 2e^{-} , \tag{6}$$

where O_v is the oxygen vacancy.

Since the films are made by oxidizing a zinc film at elevated temperatures, it is probable and will be assumed here that an excess of zinc atoms are trapped as interstitials in the ZnO lattice. This assumption has been verified by other workers for similar samples where an interstitial density of $8 \times 10^{17}/cm^3$ was determined [Ref. 4].

With excess zinc, the dominant contributors to electronic behavior are: (1) zinc donors in interstitial sites, (2) oxygen vacancy donors, and (3) oxygen interstitial acceptors. The donors predominate and the

conductivity is electronic or n-type. The fact that zinc oxide is an n-type semiconductor has been reported by numerous workers who used Hall effect measurements [Ref. 1].

From the laws of mass action, the association rate must equal the disassociation rate. For interstitial Zn, the disassociation process is

$$\frac{\text{Disassociation}}{\text{cm}^3\text{-sec}} = \frac{1}{\tau} \cdot N_{Zn_i^\times} \, . \tag{7}$$

The association process is

$$\frac{\text{Association}}{\text{cm}^3\text{-sec}} = \gamma \; n \; N_{Zn_i^+} \, . \tag{8}$$

In the above equations τ is the lifetime of the undisassociated zinc, $N_{Zn_i^\times}$ is the number of zinc atoms, γ is the recombination coefficient for the Zn_i^+ and the electron, and n is the electron concentration. Since the disassociation rate at equilibrium is equal to the association rate

$$N_{Zn_i^\times} = n \; \gamma \; \tau \; N_{Zn_i^+} \, , \tag{9}$$

or

$$K_D \; N_{Zn_i^\times} = n \; N_{Zn_i^+} \, , \tag{10}$$

where K_D is the mass action constant.

It can be shown that [Ref. 5]

$$K_D = \frac{1}{2} N_c \; \exp\text{-}\left[\frac{E_d}{kT}\right] \tag{11}$$

where E_d is the disassociation energy of the donor, and N_c is the effective density of states in the conduction band. Below the melting point it is assumed that the total number of zinc atoms is constant:

$$N_{Zn_i} = N_{Zn_i^+} + N_{Zn_i^\times} \, . \tag{12}$$

Combining Eqs. (10) and (12) gives

$$N_{Zn_i}^{+} = N_{Zn_i} \left(\frac{1}{1 + \frac{n}{K_D}} \right) . \tag{13}$$

For simplicity let $N_{Zn_i}^{+} = N_D^{+}$ which gives:

$$N_D^{+} = N_D \left(\frac{1}{1 + \frac{n}{K_D}} \right) . \tag{14}$$

A similar argument can be used for acceptors to give [Ref. 5]

$$K_A = \frac{1}{2} N_V \exp\left(\frac{E_A - E_g}{kT} \right) \tag{15}$$

and

$$N_A^{-} = N_A \frac{1}{1 + \frac{p}{K_A}} , \tag{16}$$

where N_A is the acceptor density, N_V is the density of states in the valence band, p is the hole concentration, and E_A is the activation energy. These expressions are valid for $n << N_C$ and $p << N_V$. See Fig. 13 for a sketch of the energy band picture.

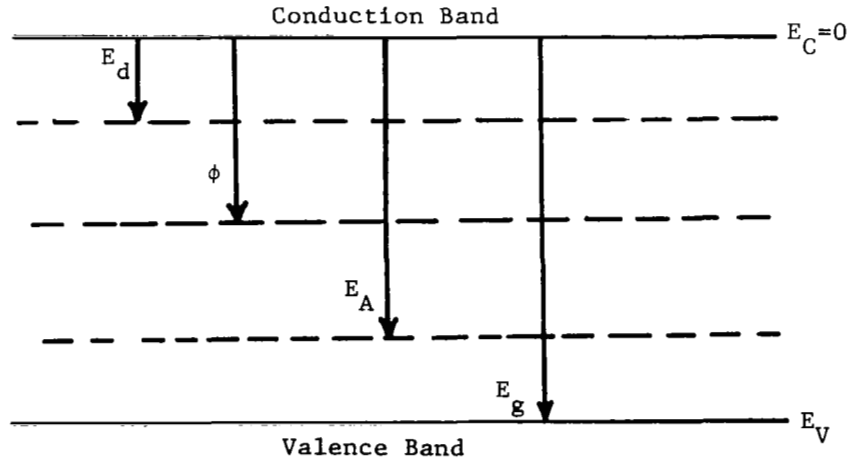

Figure 13. Band Model

Invoking charge neutrality gives

$$N_A^- + n = N_D^+ + p \ . \tag{17}$$

The electron concentration, n, is given by

$$n = N_C \exp(\phi/kT) \ , \tag{18}$$

where ϕ is the Fermi energy. The hole concentration is

$$p = N_V \exp\left[-\frac{\phi - E_g}{kT}\right] \ , \tag{19}$$

where E_g is the energy gap.

Combining Eqs. (14), (16), (17), (18), and (19) gives

$$N_C \exp\left(\frac{\phi}{kT}\right) - N_V \exp\left[-\frac{\phi - E_g}{kT}\right] - \frac{N_D}{1 + 2\exp\left[\frac{\phi + E_d}{kT}\right]} + \frac{N_A}{1 + 2\exp\left[-\frac{\phi - E_A}{kT}\right]} = 0 \ . \tag{20}$$

Equation (20) describes the Fermi energy for both donor and acceptors in the sample. Needless to say, Eq. (20) is very complex to solve for ϕ. Once ϕ is obtained, however, it can be used to evaluate p and n which are two of the factors needed in describing the conductivity.

Several special cases are of interest here.

Case A. - Near intrinsic which occurs when the number of donors canal the effects of the acceptors or at high temperatures where the donors and acceptors are not important. From Eq. (20) it is seen that if $p = n$, assuming $N_C \simeq N_V = N$, ϕ is equal to $E_g/2$. This gives

$$p = n = N \exp-\left[\frac{E_g}{2kT}\right] \ . \tag{21}$$

If ϕ is several kT below E_d and above E_A, i.e., all impurities are ionized, Eq. (20) becomes

$$N \exp(\phi/kT) - N \exp\left[-\frac{\phi - E_g}{kT}\right] - N_D + N_A = 0 \ . \qquad (22)$$

Combining Eqs. (18) and (19), and (20) and (22) gives

$$n + p = 2\sqrt{\left(\frac{N_D - N_A}{2}\right)^2 + \left(N \exp\left(\frac{-E_g}{2kT}\right)\right)^2} \ . \qquad (23)$$

If the hole and electron mobilities are assumed to be equal then the electrical conductivity becomes

$$\sigma = 2q\mu\sqrt{\left(\frac{N_D - N_A}{2}\right)^2 + \left(N \exp\left(-\frac{E_g}{2kT}\right)\right)^2} \ . \qquad (24)$$

Case B. - Heavy compensations where N_D and N_A differ only by a few percent with N_D the larger and not completely ionized. In this case, combining Eqs. (18) and (20) gives

$$n \simeq \frac{N_D - N_A}{1 + (N_A/2N) \exp(E_d/kT)} \ . \qquad (25)$$

When Eq. (25) is valid, p may or may not be negligible, depending on the difference between N_D and N_A and their magnitudes. As can be seen in Eq. (25), n will saturate with temperature to the value $N_D - N_A$. By making use of Eqs. (24) and (25) the conductivity can be plotted over its entire range. Actually N is equal to $2\frac{(2\pi mkT)^{3/2}}{h^2}$ which is temperature dependent. Compared to the exponentials, the $T^{3/2}$ dependence is negligible. Using Eqs. (24) and (25) one sees that as temperature increases from some low value, a plot of the log of conductivity versus reciprocal temperature will increase with a slope of E_d, saturate to $N_D - N_A$, and then increase at a slope of $E_g/2$.

Comparison with Experiment. - The preceding discussion is sufficiently general to apply to zinc oxide or any other semiconductor. A comparison of the experimental equilibrium data with the theoretically predicted slopes shows there are some comparisons. For example, at high temperature (region I of Fig. 1) a comparison shows that the films should have a band gap of approximately 2 eV. This value agrees with data obtained by optical means [Ref. 6].

Below the intrinsic region (region II of Fig. 1) the films show decreasing conductivity with increasing temperature. In this same range the theory predicts a steady state or saturated conductivity. Actually the mobility decreases with increasing temperature in this temperature range, however, the magnitude is not enough to explain the effects observed [Ref. 6]. In this region the experiment differs, therefore, from the theory.

At still lower temperatures, the film conductivity decreases again as predicted by the theory. However, the slopes are different for the film depending on whether or not it is in oxygen or nitrogen. In nitrogen the slope corresponds to a donor energy of 0.14 eV. The 0.14 eV has been measured by other workers in single crystals of zinc oxide as well as in films and has been identified as the zinc activation energy.

The general semiconductor theory seems to hold for high temperatures (intrinsic) at equilibrium and at low temperatures (donor dominated) for nitrogen environments. It does not hold in the intermediate temperature range nor is it valid for the low temperature oxygen environment. The almost constant slope exhibited for the total range in the transient case is slightly lower than the energy gap.

An explanation of these anomalous results must be explained by mechanisms other than that exhibited by simple semiconductors. Some possibilities are given in the following discussion. The unexpected negative temperature coefficient of conductivity (region II of Fig. 1) is considered first and is called a modified general model. Then the influence of oxygen on the conductivity is considered. Two different models are presented for the oxygen influences: (1) oxygen diffusion into the bulk, and (2) surface adsorption of oxygen resulting in electron robbing from the bulk.

Modified General Model. - The negative temperature coefficient of conductivity (region II of Fig. 1) can be explained if the acceptor concentration N_A is temperature dependent. In other words N_A will be allowed to vary with temperature.

Using Eqs. (24) and (25) and permitting the acceptor concentration N_A to vary with temperature the observations in nitrogen can be consistently explained. For the steady state observations at the higher temperatures near intrinsic (region I) and near the minimum conductivity (region II) one obtains from Eq. (24)

$$\frac{d\sigma}{dT} = - \frac{(q\mu)^2}{\sigma} \left[\left(\frac{N_D - N_A}{2} \right) \frac{dN_A}{dT} - \frac{E_g N}{kT^2} \exp(- E_g/2kT) \right] . \qquad (26)$$

Clearly in the intrinsic region $d\sigma/dT$ is positive or given in the usual manner as $d\log\sigma/d(1/kT) = - E_g/2$. Also there is a minimum at a given temperature defined by $d\sigma/dT = 0$.

At temperatures below the minimum, the slope is defined by the difference in the donor and acceptor concentrations and the rate of change in the acceptors with temperature. In this temperature range zinc oxide is n-type. Therefore, $N_D > N_A$ and we are forced to admit an increase in N_A with increasing temperature to obtain the negative slope as observed. The acceptor concentration increasing with increasing temperature in the N_2 environment must be related to the disassociation and rearrangement processes previously discussed. The diffusion of dissolved oxygen into interstitial sites is one possibility. Admittedly this is a tenuous assumption since we have no direct measure of such an effect or that it would be reversible. Another possibility is vacancy formation due to thermal disassociation of the zinc oxide lattice. From the present data, a definitive statement concerning the nature of the change in acceptors with temperature cannot be made. However, the agreement at lower temperatures between the proposed model and the observations provides major support for extending the analysis to higher temperatures.

In the low temperature range, the measured activation energy corresponds to reported values for the reaction, $Zn \rightleftarrows Zn^+ + e^-$. Analytically, this can be treated using Eq. (25). At temperatures where $2N_C/N_A >> \exp E_D/kT$ one obtains

$$\frac{dn_o}{dT} = -\frac{dN_A}{dT} + \frac{(N_D - N_A)\, N_A E_d}{2kT^2\, N_C} \exp(E_d/kT) \quad . \tag{27}$$

Again when $n_o \simeq N_A$ (region II) the slope of conductivity versus temperature is negative. Over a limited temperature range in region II the decrease in conductivity, hence the increase in acceptor concentration, follows an Arrenhius plot and provides some confidence in a thermal activation process such as

$$N_A = N_{Ao}\, e^{-\varepsilon_A/kT} \tag{28}$$

to describe the average acceptor density. The energy ε_A is the energy of formation for N_A. From Eq. (27) the maximum in conductivity with temperature can be obtained using $dN_{Ao}/dT = 0$. Using Eqs. (27) and (28) and assuming $N_D > N_A$ the peak should occur at

$$(kT)_{max} = E_o \Big/ \log\left(\frac{2N_C E_A}{N_D E_d}\right) \quad . \tag{29}$$

In region III, the nitrogen environment data can be explained in a consistent manner using Eq. (25). When $N_A/2N \exp(E_d/kT) > 1$ the usual result $d\log\sigma/d(1/kT) = - E_d$ is obtained. From Fig. 3, this turns out to be 0.14 eV in agreement with published values. From the results in Fig. 3, the conductivity of the sample has been estimated to be $.5(\Omega\text{-cm})^{-1}$ at 316°K. Using a mobility of 200 cm^2/volt-sec the free electron concentration is $5 \times 10^{16} cm^{-3}$. Using Eq. (25), the ratio N_D/N_A is equal to 1.14, assuming the value $N = 10^{19} cm^{-3}$. Therefore, a 14% compensation is realized in the bulk zinc oxide films as prepared using the oxidation technique.

The donor concentration N_D can be estimated using Eq. (29) where

$$N_D = \frac{2N_C E_A}{E_d} \exp - (E_d/kT)_{max} . \qquad (30)$$

Assuming $\varepsilon_A \gtrsim 2$ eV, one obtains $N_D \gtrsim 10^{19} cm^{-3}$. Therefore, about 1 part in 10^4 of the deposited zinc was not oxidized during the high temperature treatments.

By modifying the general theory to account for a temperature dependent acceptor density, it is possible to explain the dependence of conductivity on temperature if time is allowed for equilibrium to be reached following any changes. The transient conductivity-temperature data is also consistent with the above theory. When temperature is rapidly changed, the acceptor density is frozen in at the last equilibrium point. Therefore, the transient behavior is dominated by the previous history of the film.

As an example, if a film is in equilibrium in the intrinsic region (region I) and if the temperature is rapidly decreased, the acceptor density would remain at the high value set at the higher temperature. This would compensate the sample making it appear intrinsic to much lower temperatures than it would if the samples were allowed to equilibrate. In other words the sample would appear to be much heavier compensated. If the sample were at a low temperature having been slowly cooled from the intrinsic region and were suddenly heated up, it would behave as if it were heavily compensated in region II (no negative slope). The negative slope in this case can only result from mobility effects. These predictions are born out fairly well as shown in Fig. 8 for the transient case.

The modified general model as presented can account for the case of bulk material in non-oxidizing environments. It accounts for the negative slope in conductivity temperature plots by allowing the acceptor density to vary with temperature. Oxygen induced effects must also be accounted for and are discussed in the following paragraphs.

Diffusion Model. - In this model it is assumed that oxygen diffuses into and out of the zinc oxide film and, as a result, induces changes in the film conductivity. It is not necessary to consider the time dependence in order to develop the model, therefore, these will be discussed later. Since oxygen is the diffusant which causes the changes in the conductivity, one must consider its effects on the system. In equilibrium, the reactions for donor zinc atoms are

$$2Zn^{\times} \rightleftarrows 2ZnO - O_2(gas) \tag{31}$$

and

$$Zn^{\times} \rightleftarrows Zn^{+} + e^{-} . \tag{32}$$

Adding gives

$$2Zn^{+} + 2e^{-} + O_2(gas) \rightleftarrows 2ZnO . \tag{33}$$

If two reaction partners are of the same type, the concentration of this type occurs twice as a factor. From the law of mass action

$$(N_{Zn^{+}})^2 \, n^2 N_{O_2(gas)} = K_1 (N_{ZnO})^2 . \tag{34}$$

The concentration of zinc oxide, N_{ZnO}, is incomparably larger than all other reaction partners, therefore, it remains unchanged. Including N_{ZnO} in the constant K_1 gives

$$(N_{Zn^{+}})^2 \, n^2 = K_2 \left[N_{O_2(gas)}\right]^{-1} , \tag{35}$$

$$= K_3 \left[P_{O_2(gas)}\right]^{-1} , \tag{36}$$

where P_{O_2} is the oxygen partial pressure. From the charge neutrality condition if $n \simeq N_D$ then

$$n \simeq K_3^{1/4} \left[P_{O_2(gas)}\right]^{-1/4} . \tag{37}$$

A more realistic condition is to assume that all acceptors are ionized and only p is small compared to the other terms in the charge neutrality condition [Eq. (16)], i.e.,

$$n \simeq N_D^+ + N_A \ . \tag{38}$$

Combining Eqs. (35) and (38) gives a fourth order equation in n,

$$n^4 + 2N_A n^3 + N_A^2 n^2 - K_3 P_{O_2}^{-1} = 0 \ . \tag{39}$$

Solving for n gives

$$n = \left[\left(\frac{N_A}{2}\right)^2 + K_3^{1/2} \, P_{O_2}^{-1/2}\right]^{1/2} - \frac{N_A}{2} \ . \tag{40}$$

It has been assumed that N_A is not dependent on the oxygen partial pressure. If dependent, it can be accounted for by substituting in Eq. (40). As shown by Eq. (40), the addition of acceptors reduces the dependence of n on P_{O_2}. At low oxygen partial pressures the dependence approaches that of pure donors, Eq. (37). For comparison with the data of Fig. 2, if this model is to hold, Eq. (37) is a good approximation for most of the oxygen pressure range. It should be remembered that K_3 in this expression is temperature dependent.

If one considers another possible reaction

$$ZnO \rightleftharpoons Zn^{++} + 2e^- + \frac{1}{2} O_2(gas) \ , \tag{41}$$

then for $n = N_D$ the dependence is

$$n \propto P_{O_2}^{-1/6} \ . \tag{42}$$

In this case where it is assumed that the oxygen is allowed to diffuse into and out of the films, the film should behave in the equilibrium case in the same manner as exhibited in the non-oxygen environment previously discussed. The only difference should be a reduced conductivity magnitude.

The high and medium temperature data is consistent with the diffusion model, however, at low temperatures the data gives a slope much larger than the E_d value predicted. One could explain this large slope by postulating that a new donor level is uncovered at the expense of the shallow donors. Although possible, this seems unlikely. The diffusion model then lacks the ability to explain the low temperature conductivity data.

The transient response can be explained in oxygen by the same modified model presented for non-oxygen environments. In other words, the sample will remain intrinsic, if fast cooled from the intrinsic region. If heated from the low temperature it should not show the negative slope region.

A model has been developed by Fritzsche for the conductivity when the sample is heated and cooled in vacuum and in oxygen [Ref. 7]. The model is based on the standard semiconductor model and accounts for diffusion of oxygen using ordinary diffusion theory, i.e.,

$$D = D_o \exp(- E/kT) \ . \tag{43}$$

Fritzsche's work considers in some detail the case of constant heating and cooling rates. His model, therefore, attempts to explain the transient response of conductivity with temperature.

Surface Model. - The observed decrease in conductivity with increasing oxygen pressure could be attributed to surface effects. In this model, the oxygen adsorbed on the surface is assumed to rob electrons from the bulk. The effect is shown in Fig. 14. Assuming that O^- ions, adsorbed on the surface are separated by 3 - 10 Å, then a monolayer could accommodate greater than 10^{14} O^-/cm^2. The density of bulk free electrons per unit surface area is equal to the thickness χ $5 \times 10^{16}/cm^3$. For a one micron film, a density of 5×10^{12} electrons/cm^3 is obtained. The surface state density could therefore perturb the bulk conductance in a very significant manner.

Several schemes have been proposed which postulates the surface effect [Ref. 8]. One effect involves a disassociation process at a zinc-rich surface on which the oxygen is adsorbed and desorbed.

In any surface model the surface and bulk can be treated as parallel conductors. There is a charge depleted region as one moves away from the surface. The amount of oxygen adsorbed on the surface will be dependent on the oxygen partial pressure and the temperature. The large activation energy exhibited by the film in oxygen at low temperatures could easily result from this surface effect.

The amount of oxygen absorbed on the surface could be of the Langmuir type such that

$$N_{O_2} = \frac{aK}{P_{O_2}^{1/2} + bK} \ , \tag{44}$$

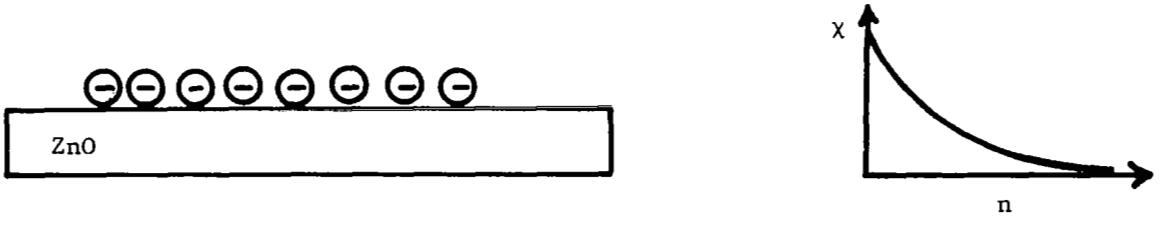

Figure 14. Surface Model

where a, b, and k are constants and may be temperature dependent. Models of this type and others have been discussed in the literature by other workers [Refs. 1, 8, 9].

SECTION III

SENSOR DESIGN AND CONSTRUCTION

Sensor Head

In designing and fabricating a laboratory model partial pressure oxygen sensor, two design concepts for heating the film were planned during early stages of this work. The first was to use a single composite structure for the heater, zinc oxide film, and film substrate which could be encased in a suitable insulated housing. The second design would include separate construction of a heater and film substrate which could be assembled. The latter design enables one to test many sensor films with one heater and also replace a defective sensor or heater should it fail. The heater for both designs was cylindrically shaped with the film substrate completely surrounding the heater. Basically, the heater construction was the same for both composite sensor structure and the assembled sensor. Photographs of a typical composite sensor and one with removable heater are shown respectively in Figs. 15 and 16.

The heaters for the zinc oxide films were constructed using nichrome wire as the heating element. The wire was wound onto a threaded ceramic cylinder. The cylindrical ceramic base for supporting the wire was machined from unfired lava using a lathe. The diameter of the heaters were 1/8 to 1/4 inch with lengths 7/16 to 1 inch. Next, the lava was threaded (60 or 72 threads per inch) in order to maintain proper spacing for the nichrome windings and to enhance uniform heating of the thin film sensor which would be applied in a latter process. The threaded lava cylinder was fired in an oven with the temperature increasing at 200°F per hour until reaching 2000°F and remaining at that temperature for approximately 30 minutes. The heater base was cooled at the same rate. From this point, the sensor construction differs for the two conceptual designs.

For the composite design, the heaters were coated by dipping in porcelain cement (several types were used) after winding the heaters with nichrome wire. An air drying cement, oven fired, and chemical setting cements were tested. After drying or firing of these various coatings, the surface was much too porous and rough for applying satisfactory thin films of zinc. An attempt was made to improve the surface finish glazing the ceramic. Although several materials were used, none resulted in sufficiently smooth surfaces. An additional requirement was to match thermal expansion coefficients of expansion of the zinc oxide film and the glass coating from room temperature to the 600°C necessary for oxidizing the zinc film.

Further study and experiments with various materials and techniques will be necessary in order to develop a composite structure. It would, however, enable further reduction of weight and power requirements.

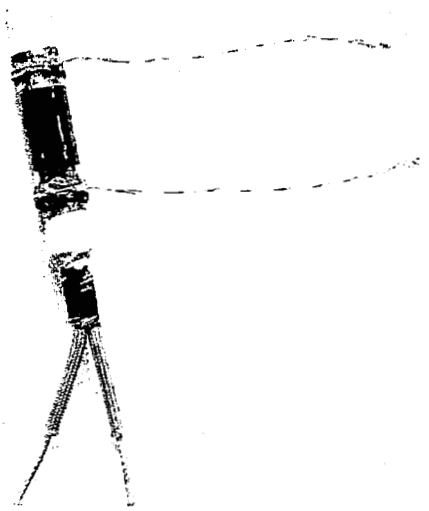

Figure 15. Photograph of a Typical Oxygen Sensor with Composite Construction

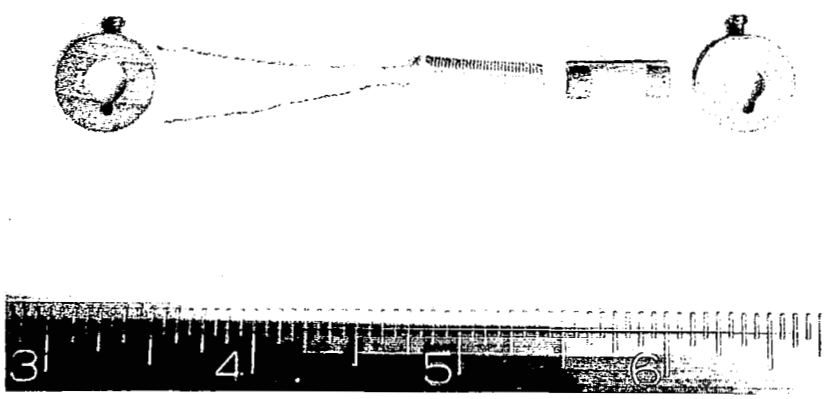

Figure 16. Oxygen Sensor with Substrate and Removable Heater

The assembled sensor head design has an advantage over the composite design in that the entire unit including heater and substrate need not experience the high temperatures of oxidation required for forming the oxide films. The discrete component structure enables evaporation and oxidation of the film before mounting on the heater. In the laboratory, it also permits one assembly to be used with many zinc oxide films for testing purposes.

Substrates for Laboratory Model. - Various sensor substrates, Pyrex, quartz, alumina, and several types of ceramic, were used with the zinc films. The best adherence between the film and substrate after oxidizing the zinc films at 600°C for 4 hours, was obtained with alumina and mullite. Severe peeling of the film resulted when quartz was used as a substrate. A tubular ceramic substrate with an inside diameter of 1/8 inch and a diameter of 3/16 inch for the outside with a length of 7/16 inch long was chosen. The substrates were cleaned with alconox, trichloroethylene, water, rinsed in alcohol and dried before painting bands around each end with liquid bright platinum to provide contact regions for the sensing film. These gave electrical contact to the zinc oxide which did not degrade with time as did the previously used liquid bright gold contacts. After firing the liquid bright platinum areas at 450°C in air, they were cooled at approximately 100°C per hour.

After removing the tubular substrates from the oven, they were rinsed in alcohol before being placed in a vacuum evaporation system for depositing the zinc film. Zinc films were prepared in thicknesses ranging from 500 to 1000 Å with a maximum pressure of 10^{-4} torr. The condensation rate of the zinc on the substrate is very dependent upon the substrate temperature and previous surface treatments. The surface treatments include precoating the surface with a thin (< 100 Å) silver layer to enhance uniform condensation of the zinc. Evaporations have been performed successfully without this precoating of silver; however, some substrates showed regions of nonuniform thickness for both cooled and uncooled samples. In addition to precoating, the lowering of substrate temperatures (< 20°C) proved useful in obtaining uniform films. The sleeves were inserted over rods approximately the inner diameter of the sleeves and were attached to a cold plate cooled with liquid nitrogen. The zinc concentrically coated the ceramic substrate without any necessity for rotating the substrate during the evaporation. The zinc was evaporated from either a porcelain crucible or a tungsten boat.

After evaporation of the zinc film, it was placed in an oxygen filled tube furnace and heated at a rate no greater than 300°C per hour to a maximum of 600°C and maintained at that temperature for a period of 4 to 8 hours depending on film thickness. A cooling rate of less than 200°C per hour was used to return to room temperature. Slow heating and cooling prevents the zinc oxide film from cracking due to the different thermal expansion coefficients between film and substrate. The oxidation process was considered complete when the films appeared semi-transparent upon the mullite tubes.

Several techniques were investigated for electrical lead attachment to the oxygen sensing film. First attempts to attach the leads used a conductive glass with a silver filler and flow solder techniques. These attempts were unsuccessful for long term operations. The conductive glass available was fired at 425°C and operated at 400°C which probably caused the silver to migrate from the conductive glass leaving it almost non-conductive. These contacts deteriorated or failed after a period of between one or two weeks after initial operation.

Using pressure contacts to attach electrical leads was successful. A small ceramic collar just large enough to fit over the mullite tube was threaded so that a set screw applied pressure to an electrical lead. Using this, gold wires were first used for electrical leads; however, they degraded and failed. Upon moving the gold wire to a new region of the fired-on platinum a good contact to the film resulted but this would also degrade. This indicated that the gold wires were probably producing an intermetallic compound at the gold and platinum interface at the elevated temperatures. The gold wire was replaced with one made of platinum and no failures have been observed during testing periods of approximately two months.

The insulated housing for the sensor was constructed using a double wall glass structure similar to a miniature thermos bottle. The inner walls of the housing were coated with silver to reduce the heat loss. After coating with silver the space between the inner walls was evacuated to achieve better insulation and thus reduce heat loss from the sensor heater. The gas inlet and outlet tubes were welded together to reduce heat loss by enhancing heat transfer to the incoming gas. The inlet tube was extended approximately 2 cm into the sensor housing to permit most of the gas to pass across the sensing film as shown in Fig. 17.

In testing the sensor head at gas flow rates less than 40 cm^3 per minute the power required was between 5 and 6 watts for the heater. Power requirements could be further minimized by reducing the present sensor head size which weighs 30 gm and occupies less than 30 cm^3 space. However, for laboratory purposes the sensor head shown in Figs. 18 and 19 allowed easy access to the sensor assembly for intermittent inspection during evaluation tests. Once preliminary testing was completed, the glass enclosure was sealed to the electrical feedthrough.

The oxygen partial pressure sensor depends for its operation on oxygen induced changes in the resistance of zinc oxide. In order for the film to respond to oxygen pressure changes in reasonable times, the film must be maintained at a constant elevated temperature. This requires a temperature controller.

The temperature controller utilizes a platinum resistance thermometer in a bridge circuit. The calibration curve of the platinum resistance thermometer is shown in Fig. 20. The bridge output is applied to a differential amplifier which supplies a potential for controlling the current through the heater and thus controls the temperature of the sensing film.

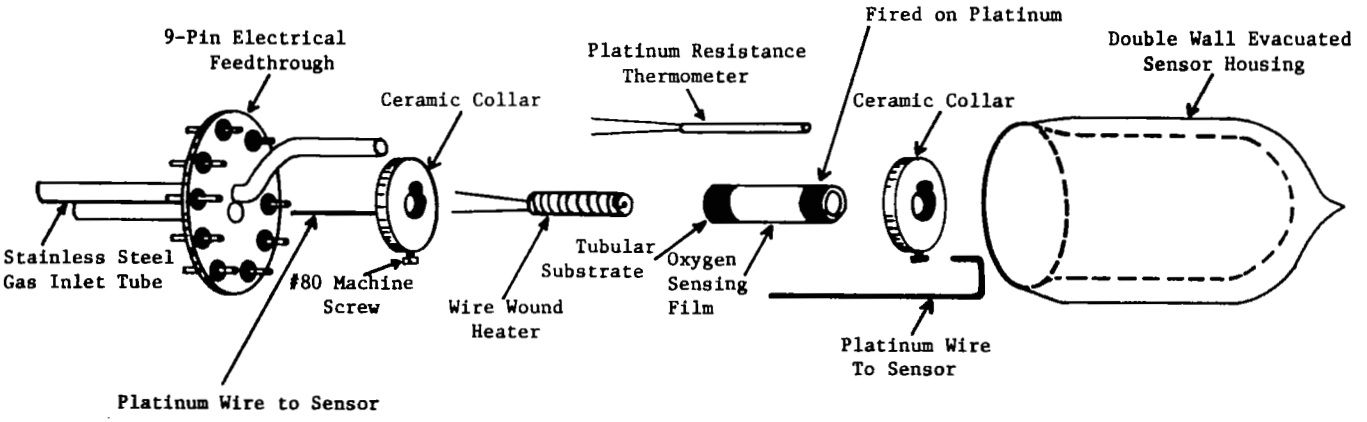

Figure 17. Sensing Head

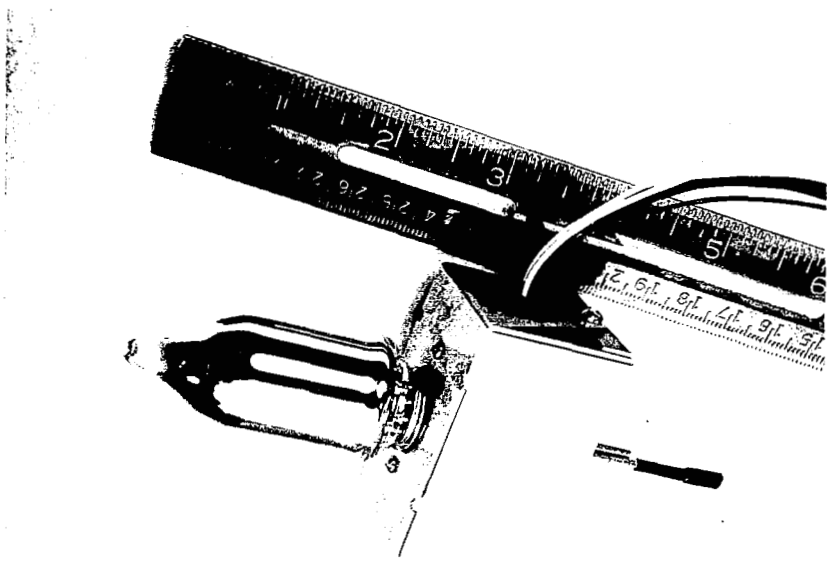

Figure 18. Photograph of Oxygen Partial Pressure Sensor Head

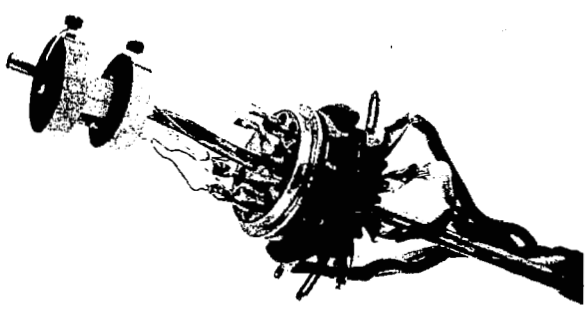

Figure 19. Photograph of Oxygen Partial Pressure Sensor Head with Insulated Housing Removed

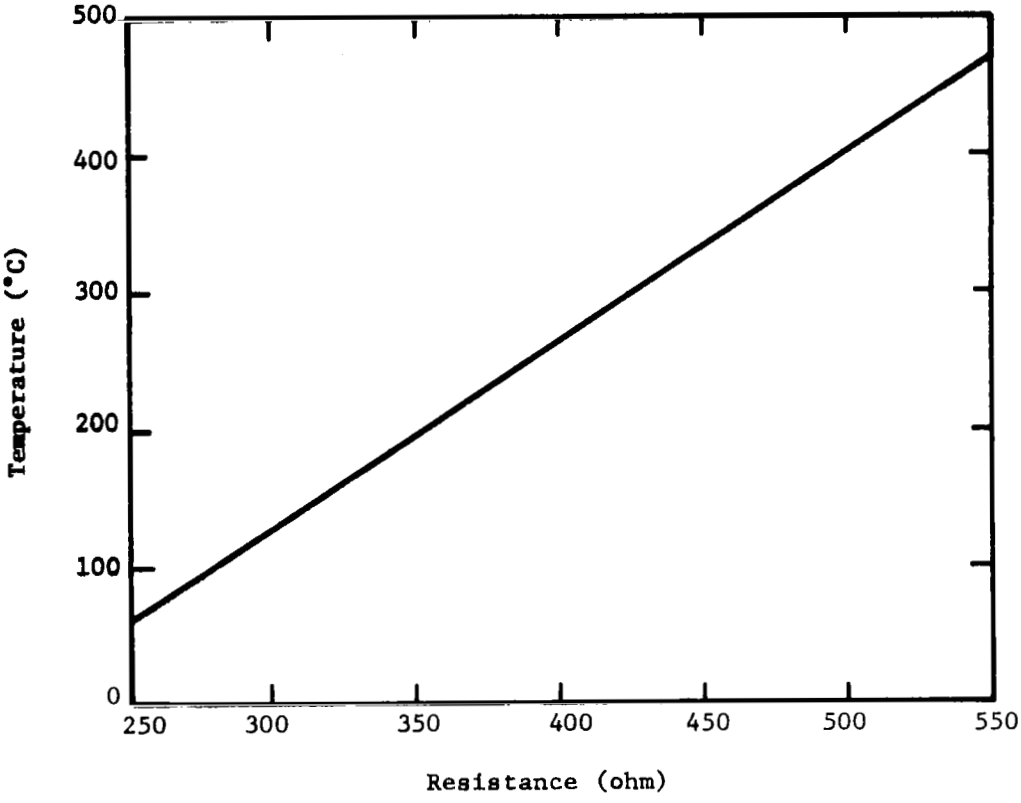

Figure 20. Platinum Resistance Thermometer Calibration Curve

A simplified schematic is shown in Fig. 21 and a complete diagram in Fig. 22. At present, the heater requires about 5.5 watts to maintain a temperature of 400°C. The total power required for the entire unit, including the heater and temperature controller is approximately 8 watts.

Sensor Operation

In using the zinc oxide film as an oxygen sensor, its electrical conductivity must be monitored while maintaining the film at an elevated temperature. In selecting the optimum temperature for sensor operation, one must consider the power available to heat the sensor, accuracy in controlling temperature, an acceptable time response of the sensor, as well as the electrical conductivity variation for the oxygen partial pressures of interest. It is desirable to operate the sensor at temperatures exceeding 200°C to achieve reasonable response times.

At this point it is desirable to discuss some general experimental observations before defining and stating the actual response times encountered with the sensor.

The experimental technique for testing the sensors at various partial pressures will be described in a later paragraph. In using the various mixtures of oxygen and other gases such as nitrogen, helium, argon, and carbon dioxide, the time required for the electrical conductivity to reach a steady state value decreased with increasing concentrations of oxygen in the mixture. The time response of the sensor changed a very small amount as the mixture flow rate was varied indicating a small dependence upon the temperature of the gas in the vicinity of the sensor. This variation in response time was observed with the sensor temperature remaining constant. The times required to reach equilibrium for a change from nitrogen to oxygen and a change from oxygen to nitrogen are shown respectively in Figs. 5 and 6.

In selecting the operating temperature of the sensor, it is informative to observe the conductance versus reciprocal temperature plotted in Fig. 1. In consideration of response times below temperatures of 200°C, it was desirable to operate the sensor beyond the first maximum of the electrical conductance. In considering the difficulty and additional circuitry for controlling the temperature within very narrow limits, the ideal temperature for operation is when $\frac{\Delta G}{\Delta T}$ is approximately zero. The sensor operating temperature was chosen at approximately 400°C as a compromise between time response of the sensor and the strict requirements for controlling the temperature.

Laboratory Model Evaluation

The oxygen sensor models were tested at various temperatures and the response time recorded. In general, the response time of the sensors

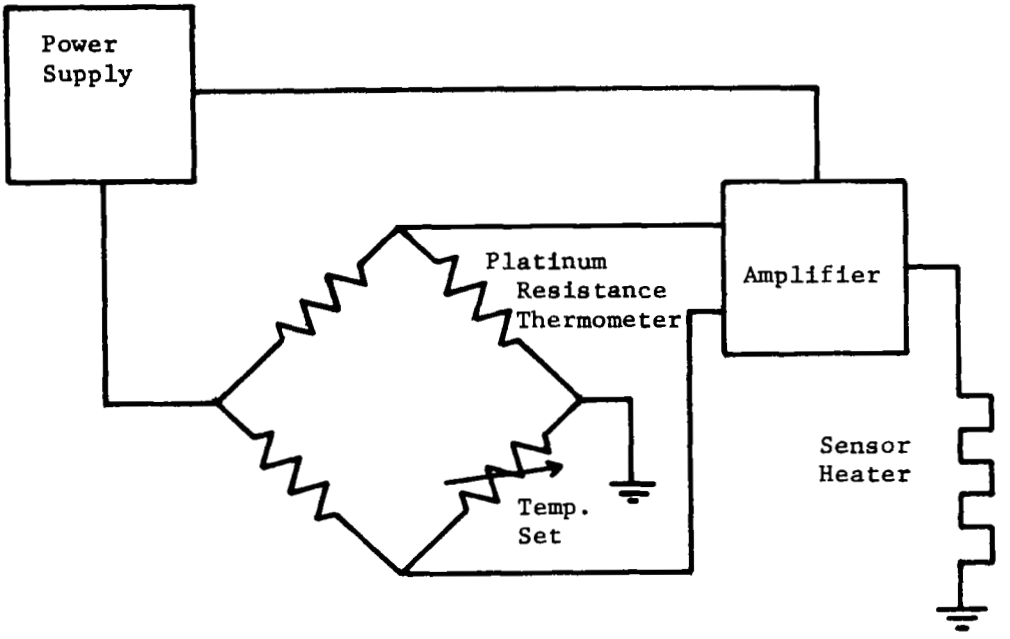

Figure 21. Simplified Schematic of Temperature Controller

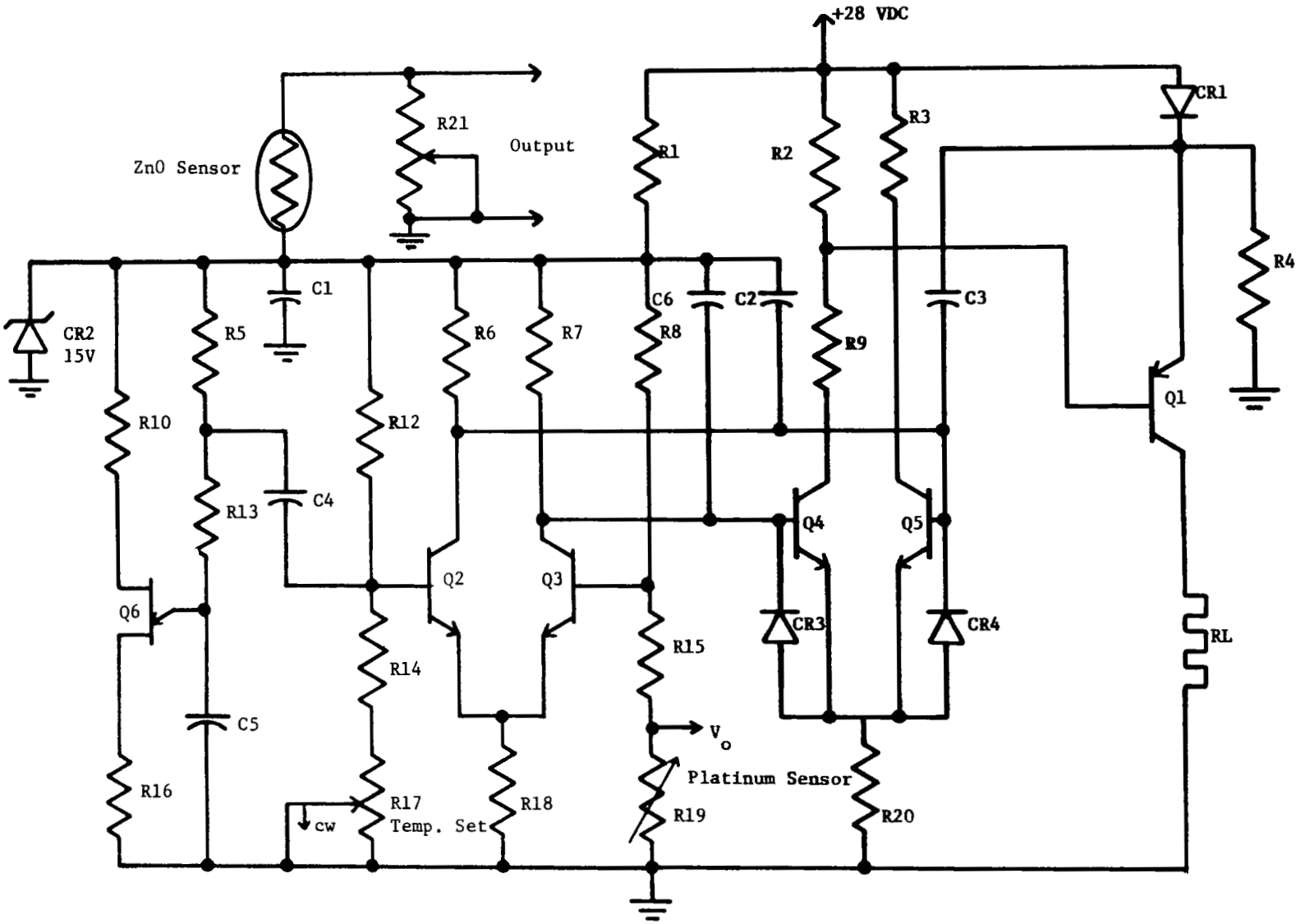

Figure 22. Schematic of Temperature Controller

Table I. Temperature Controller Parts List

Symbol		Description
R1	470Ω	2W WIREWOUND, 5%
R2	470Ω	2W WIREWOUND, 5%
R3	470Ω	2W WIREWOUND, 5%
R4	4.7K	2W WIREWOUND, 5%
R5	22Ω	1/4W, 5%
R6	2000Ω	1/8W METAL FILM, 1%
R7	2000Ω	1/8W METAL FILM, 1%
R8	3900Ω	1/8W METAL FILM, 1%
R9	470Ω	2W WIREWOUND, 5%
R10	470Ω	2W WIREWOUND, 5%
R12	3900Ω	1/8W METAL FILM, 1%
R13	12K	1/4W, 5%
R14	2000Ω	1/8W METAL FILM, 1%
R15	1820Ω	1/8W METAL FILM, 1%
R16	47Ω	1/4W, 5%
R17	500Ω	TRIMPOT, 5%
R18	1K	1/4W
R19	500Ω	Platinum Resistance Thermometer at 400°C

Symbol		Description
R20	530Ω	2W WIREWOUND, 5%
R21	50K	TRIMPOT
RL	35Ω	NICHROME HEATER
CR1	1N2068	750 mA 200V DIODE
CR2	1N9658	15V ± 5% 400mW ZENER
CR3	1N914	DIODE
CR4	1N914	DIODE
Q1	2N1038	TRANSISTOR
Q2-Q3	12A8	DUAL NPN TRANSISTOR
Q4	2N1711	TRANSISTOR
Q5	2N1711	TRANSISTOR
Q6	2N2646	UNIJUNCTION
C1	33μf	15WVDC SOLID TANTALUM
C2	.033μf	35WVDC SOLID TANTALUM
C3	.1μf	35WVDC SOLID TANTALUM
C4	.1μf	35WVDC SOLID TANTALUM
C5	.1μf	35WVDC SOLID TANTALUM
C6	.003μf	35WVDC SOLID TANTALUM

decreased for increasing temperature. Response times are plotted as a function of temperature in Figs. 23 and 24. The time required for the sensor to reach 50% of its final value is the response time shown in Figs. 23 and 24. Experimental results indicated that response times were dependent upon whether the sensor was being changed to a more or less concentration of oxygen. Figure 23 illustrates the fast time response when going from a nitrogen environment to an oxygen environment. The flow time response shown in Fig. 24 was obtained for changing the environment from oxygen to nitrogen.

The oxygen sensor has been exposed to water vapor in various mixtures of nitrogen and oxygen. A simplified flow diagram of the gas system for injecting water vapor into the mixture is shown in Fig. 25. The gas mixture and flow rate was determined by passing the individual gas through two rotameters and then directly to either the sensor housing or through a reservoir of water before entering the sensor housing. The sensing film experienced a transient effect shown in Fig. 26 lasting about 60 minutes when switching from dry gas mixture to a moist gas; however, after each successive exposure to the water vapor the transient changes became less. A few of the thicker films experienced nonreversible changes in resistance as shown in Fig. 27 when exposed to gas mixtures containing water vapor. A portion of the transient was also associated with flushing the small volume associated with the water reservoir and tubing.

In testing the oxygen sensor, commercial grades of 99.99% of oxygen, nitrogen, argon, helium, and carbon dioxide were used. The various mixtures were obtained using rotameters and controlling the individual flow rates with needle valves. Each mixture was then fed to the sensor housing at a flow rate of 30 cm^3 per minute. The absolute pressure of the gases during the sensor testing was held at one atmosphere.

The sensor prototype was tested for oxygen partial pressures ranging from 0.76 to 760 torr as shown in Figs. 28 and 29. From Fig. 28, the following sensitivity expression was obtained

$$\frac{\frac{\Delta R}{R}}{\Delta P_{O_2}} \simeq 0.2\, P_{O_2}^{-1} \,. \tag{45}$$

For example, calculating the sensitivity at 160 torr oxygen level using data shown in Fig. 28 yields

$$\frac{\frac{\Delta R}{R}}{\Delta P_{O_2}} = 1.25 \times 10^{-3}\ \text{torr}^{-1} \,. \tag{46}$$

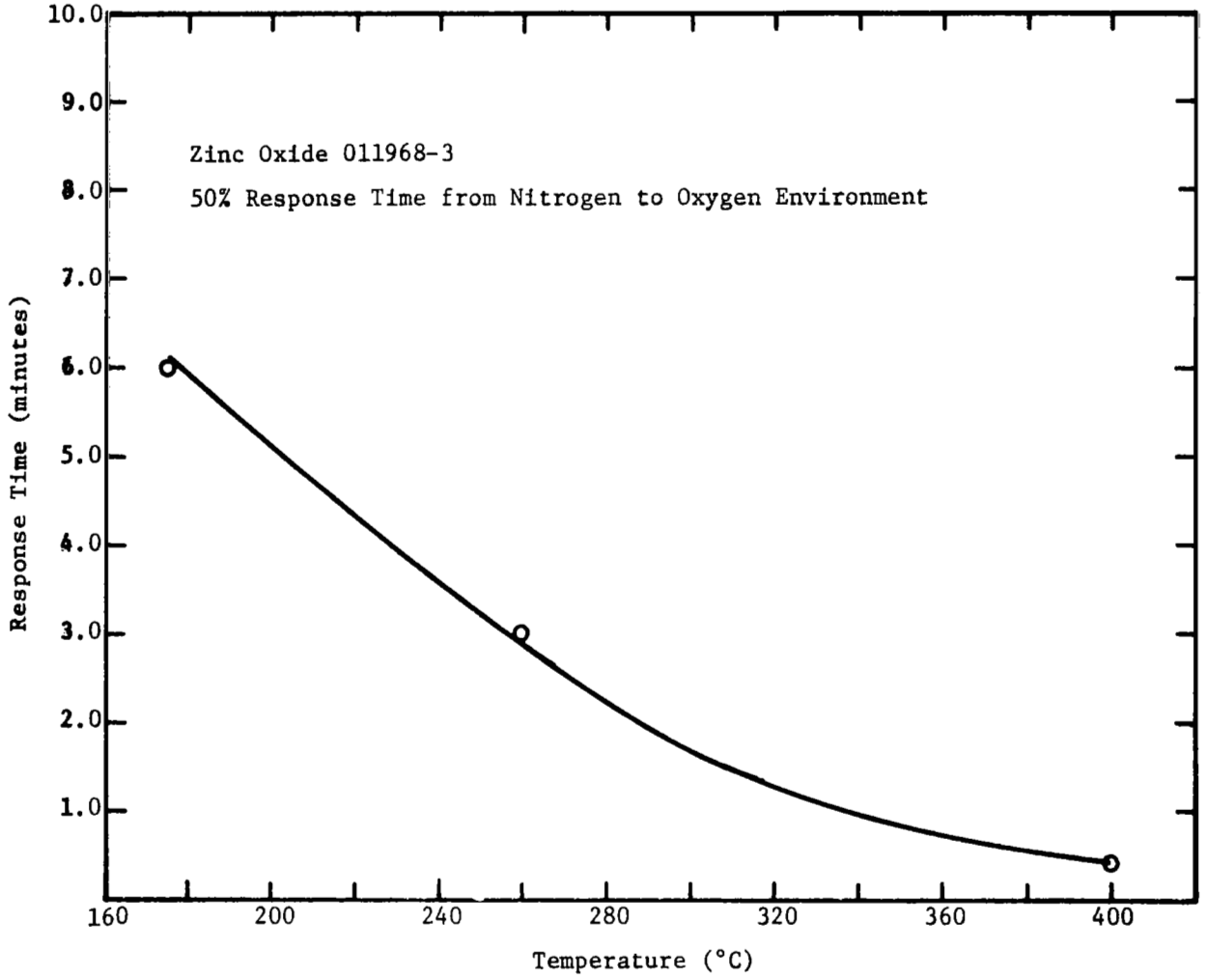

Figure 23. Response Time vs. Temperature

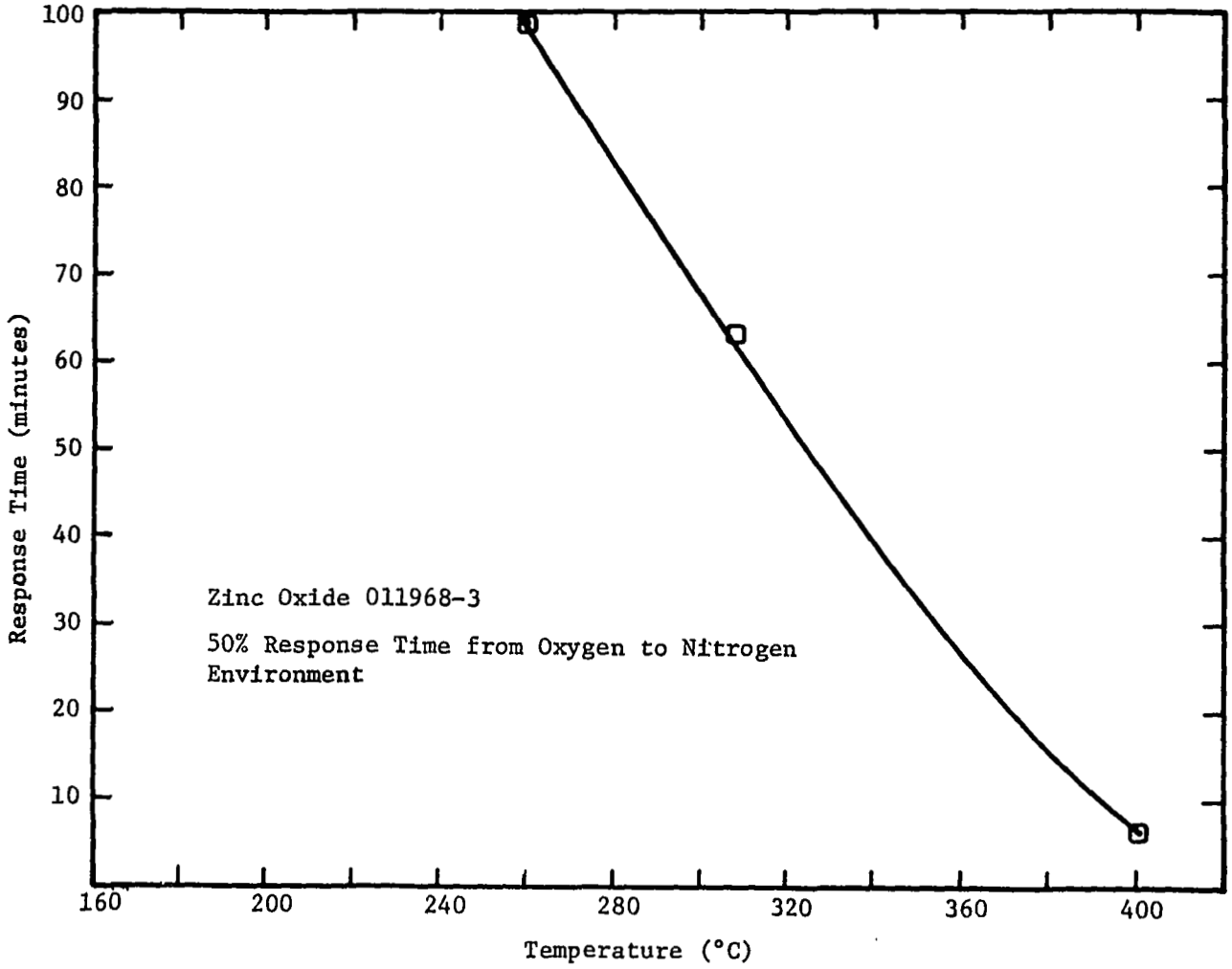

Figure 24. Response Time vs. Temperature

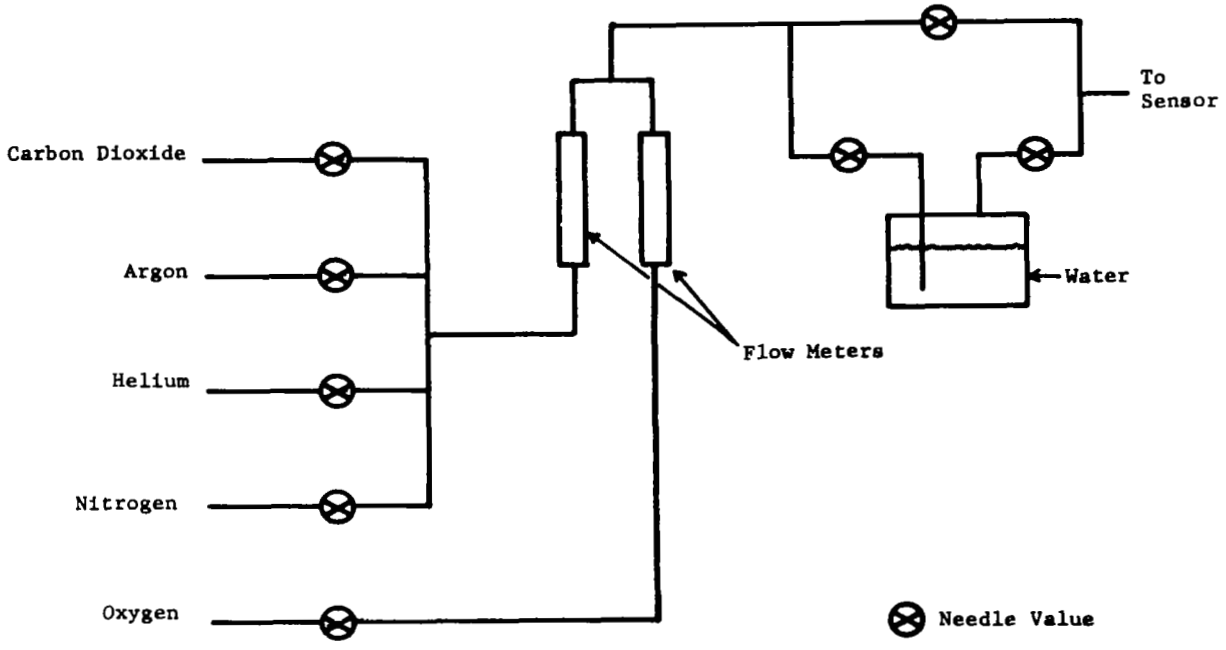

Figure 25. Diagram of Gas System

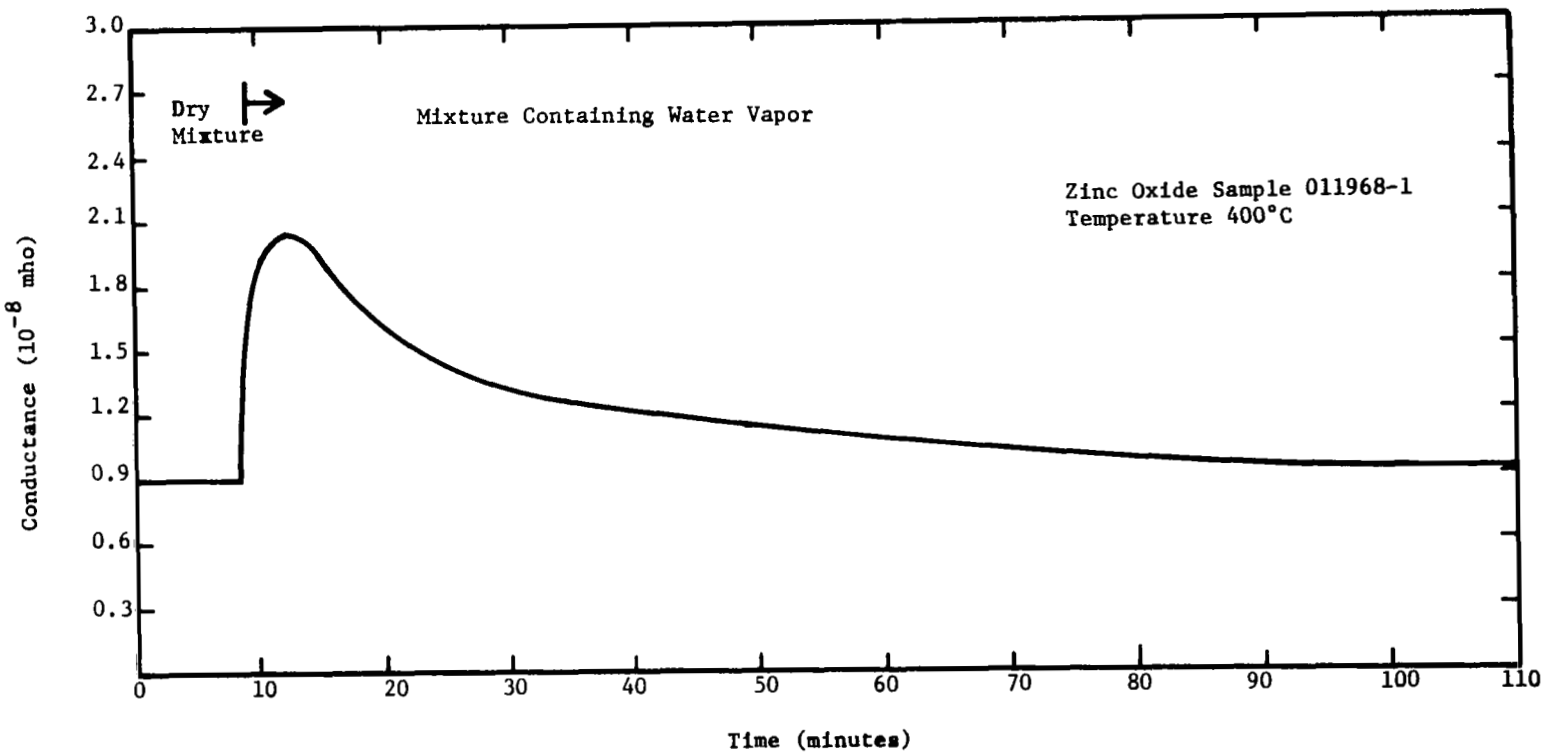

Figure 26. Sensor Response to Water Vapor

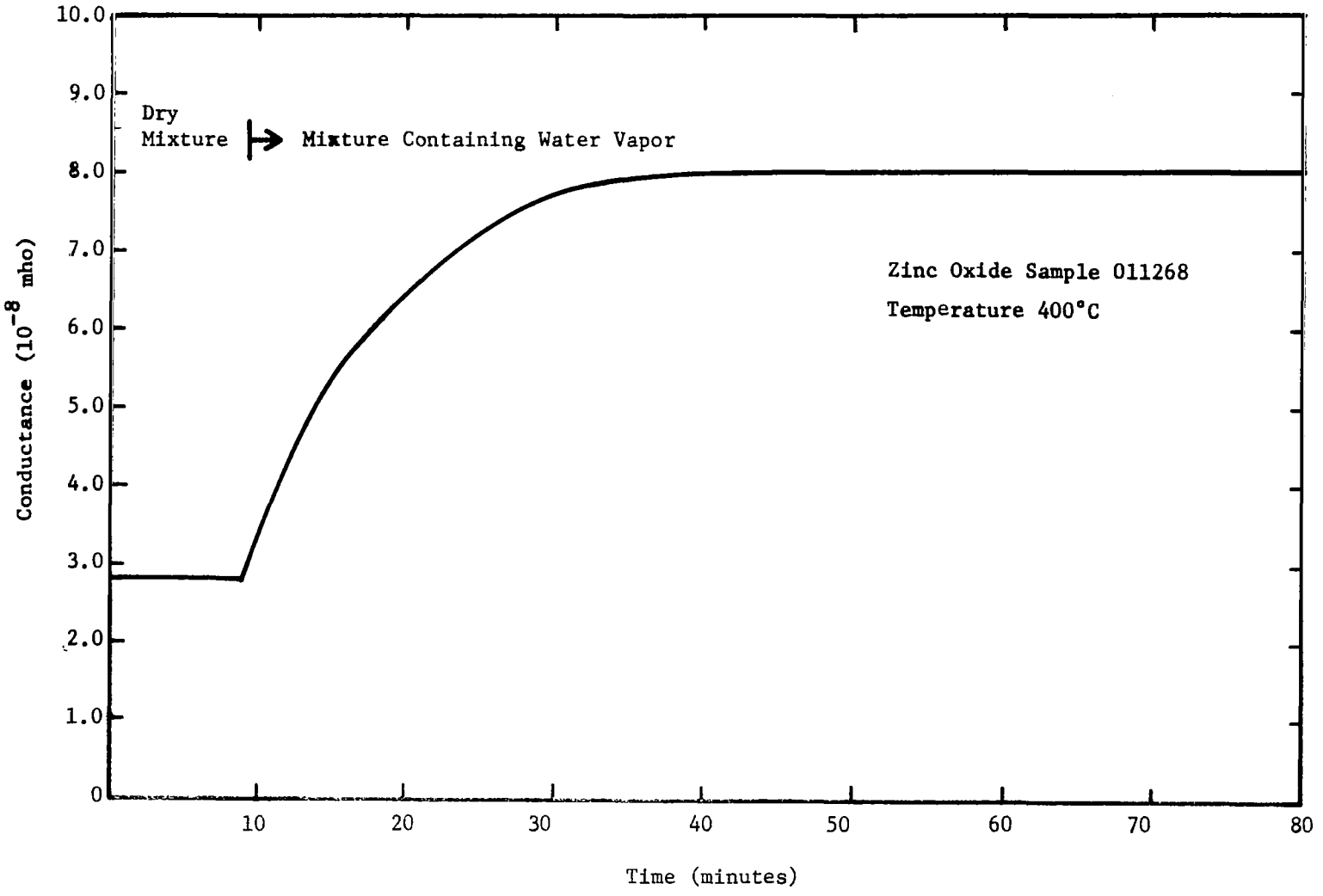

Figure 27. Sensor Response to Water Vapor

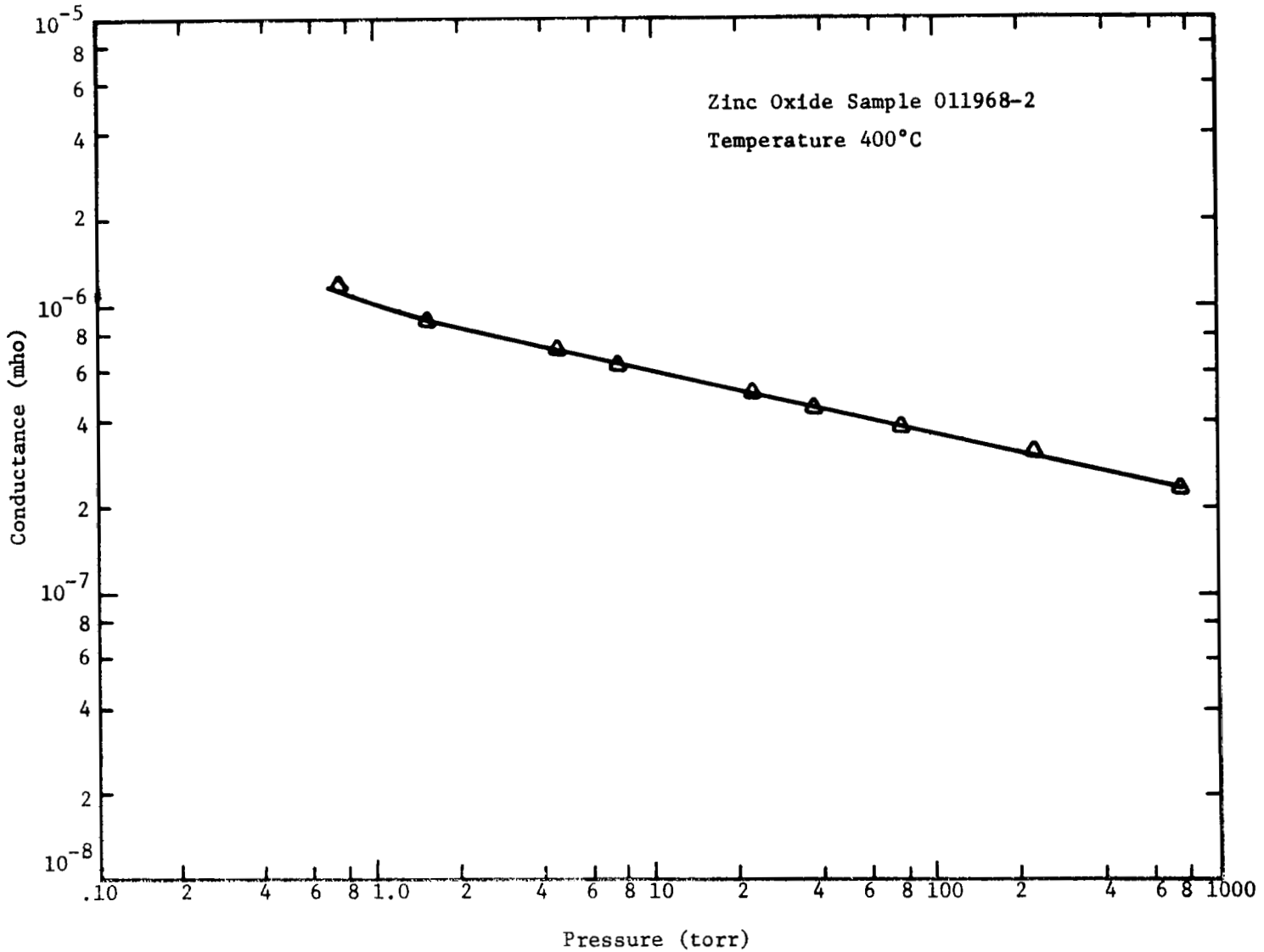

Figure 28. Electrical Conductance as a Function of Oxygen Partial Pressure

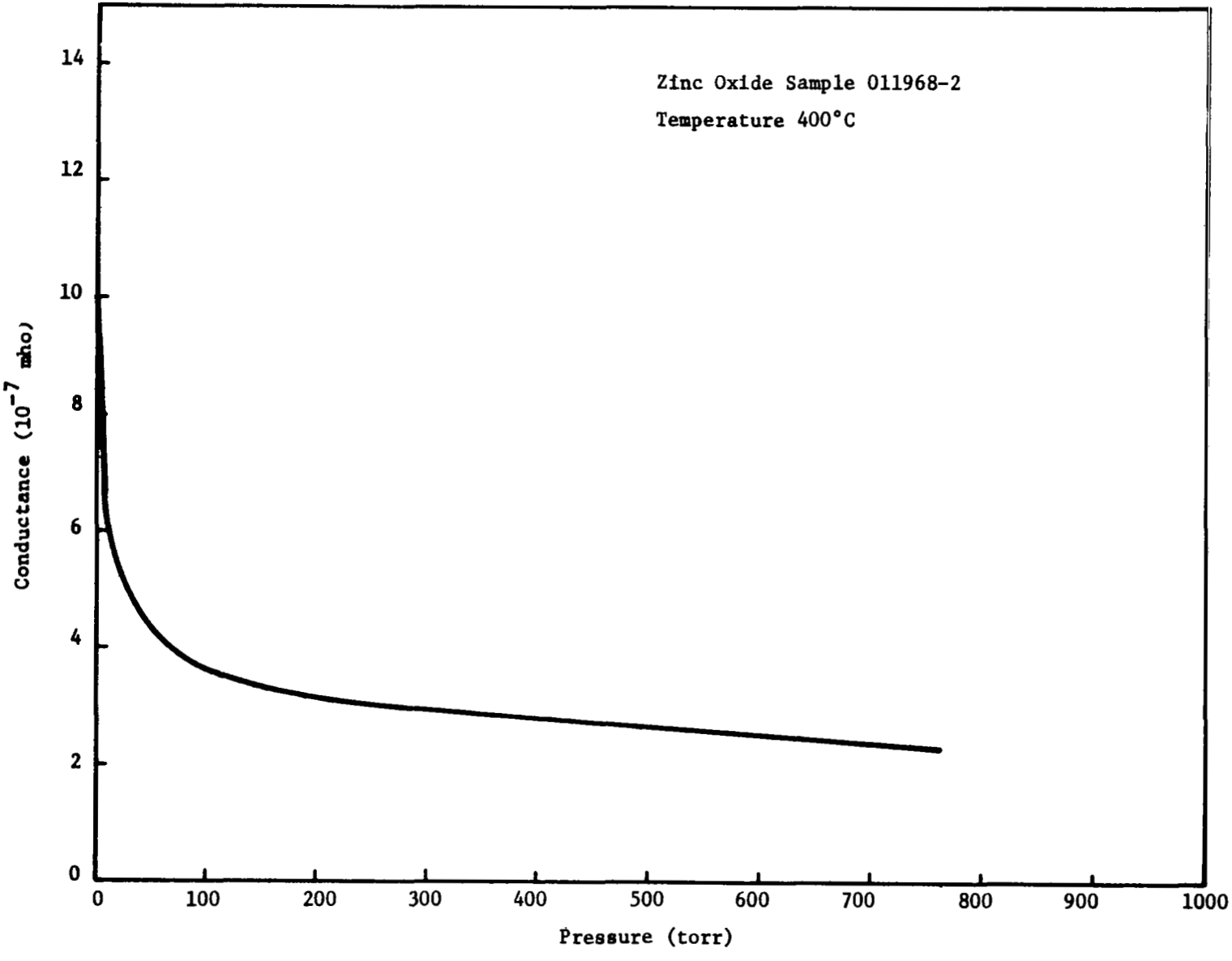

Figure 29. Electrical Conductance as a Function of Oxygen Partial Pressure

The measurements were performed using various oxygen concentrations in nitrogen. In mixing the two gases the experimental error was less than 10% for experimental data involving partial pressure of oxygen.

Because of the limited time available for testing the stability, accuracy, and reliability of the prototypes, many of these tests were performed simultaneously. As a result, the sensor experienced severe thermal cycling, unusually high flow rates, water vapor for long periods, and a variety of gas mixtures. One sensor was tested for approximately two months and another one for approximately one and one-half months. Although unknown, the sensor lifetime has been shown to exceed two months with no apparent future failure modes. No failures were observed in the prototypes tested even under the severe test conditions. The stability of one of the sensors is indicated in Fig. 30. The upper data points were obtained with the sensor in a 100% nitrogen environment at 400°C. With the same sensor in a 100% oxygen environment at 400°C, the lower data points resulted. Using this data, the worst case of stability results because of the severe thermal cycling and extreme flow rates of various gases mixed with water vapor. After correcting for barometric pressure fluctuations the maximum excursion from the mean oxygen level of 760 torr was a 37 percent increase and 9.3 percent decrease corresponding to 286 torr and 82 torr, respectively. In the absence of severe thermal cycling the stability of the transducer was approximately $\pm$ 3 percent at 760 torr oxygen level with gas mixtures containing moderate amounts of water vapor for 100 hour time periods.

The sensors were operated using a power supply for the heaters operated in a constant current mode. In laboratory testing the use of a constant current through the heater performed satisfactorily without the necessity of using a temperature controller.

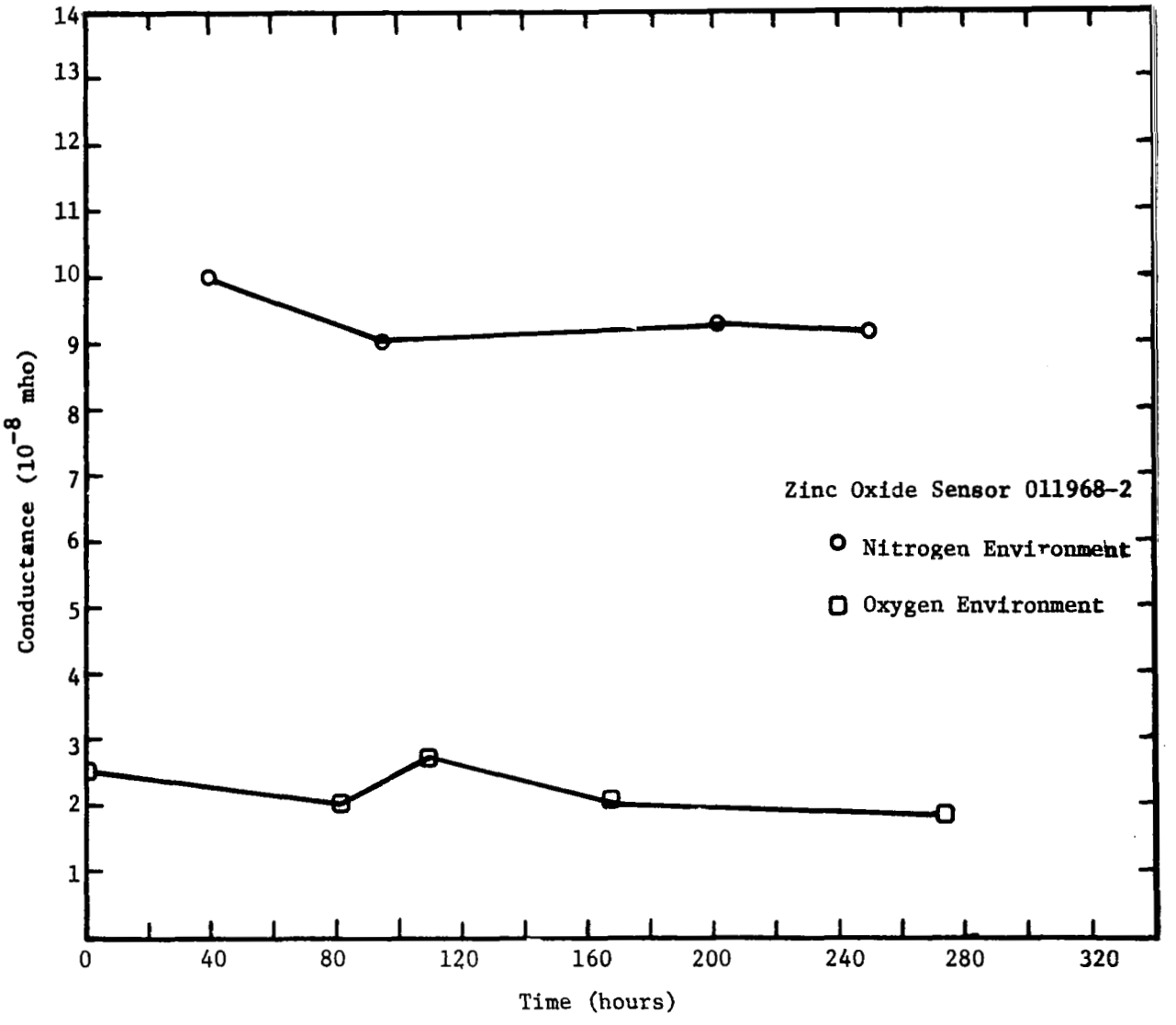

Figure 30. Plot of Sensor Stability

SECTION IV

CONCLUSIONS

The feasibility of using thin films as sensing elements for oxygen partial pressure has been investigated and a laboratory model constructed. The work has centered in two major areas during this investigation: (1) preparation and characterizing zinc oxide and tin oxide films to be used for oxygen sensing elements, and (2) designing and constructing a laboratory model suitable for evaluating thin films for sensing oxygen partial pressure.

Zinc oxide films have been successfully prepared and studied experimentally and theoretically. Using the results it has been possible to fabricate an oxygen partial pressure sensor utilizing zinc oxide films. The laboratory models proved to be rugged, stable, and offered a wide sensing range of oxygen partial pressures. They are capable of measuring partial pressures of oxygen from less than 1 mmHg to greater than one atmosphere. Time constants of approximately one minute are possible to obtain a 63 percent value of the oxygen partial pressure.

Tin oxide doped with zinc was also investigated and found to be sensitive to oxygen partial pressures at temperatures less than 300°C. The tin oxide films exhibited more instability than films of zinc oxide. The tin oxide films did, however, have much shorter response times than the zinc oxide films. Due to the difficulty in preparing the zinc doped tin oxide films and the instability associated with them, further effort in this area was discontinued in favor of the more promising zinc oxide films.

Illustrating the feasibility of using thin films as oxygen sensing elements, a laboratory model was fabricated and evaluated. The oxygen partial pressure sensor consisted of a heater, electrical readout, and temperature controller. The entire unit required approximately seven watts of power.

In testing the laboratory model, no failures were observed indicating a sensor lifetime of several months. The use of thin films as oxygen sensors make it feasible for the sensing head to be very small and lightweight. The sensing head for the laboratory model weighed approximately 30 grams and occupied 30 cm^3.

REFERENCES

1. Heiland, G.; and Mollwo, E.: "Electronic Processes in Zinc Oxide", Solid State Phys., Acad. Press, Vol. 8, pp. 193-323.

2. Holland, L.: Vacuum Deposition of Thin Films, John Wiley and Sons, Inc., New York, 1960.

3. Matthews, H. E.; and Kohnke, E. E.: "A Preliminary Study of Certain Electrical Properties of Stannic Oxide Ceramics", NASA CR-376, Prepared under Grant No. NsG-609, Oklahoma State University, Jan. 1966.

4. Bogner, G.: "Messungen Der Elecktrischen Leitfahigkeit und Des Halleffekts An ZnO Kristallen und Ihre Deutung Durch Storbander", J. Phys. Chem. Solids, Pergamon Press, Vol. 19, Nos. 3/4, pp. 235-250, 1961.

5. Spenke, Eberhard: Electronic Semiconductors, McGraw-Hill Book Co., Inc., New York, 1958.

6. Neuberger, M.: "Zinc Oxide", AD 425 212, October 1963.

7. Fritzsche, H.: "Der Einfluib Von Gelostem Sauerstoff Auf Die Elektrische Leitfahigkeit Von Zinkoxyd", Z. Physik, Vol. 133, p. 422, 1952.

8. Bevan, D. J. M.; and Anderson, J. S.: "Electronic Conductivity and Surface Equilibria of Zinc Oxide", Discussions Faraday Soc., Vol. 8, p. 238, 1950.

9. Collins, R. J.; and Thomas, D. G.: "Photoconduction and Surface Effects with Zinc Oxide Crystals", Phys. Rev., Vol. 112, No. 2, October 15, 1958.

BIBLIOGRAPHY

Baumbach, H. H.; and Wagner, C.: Die elektrische Leitfähigkeit von Zinkoxyd und Cadmiumoxyd. Z. Physikal Chem. (B), Vol. 22, 1933, pp. 199-211.

Blakemore, J. S.: Semiconductor Statistics. Pergamon Press, New York, 1962.

Bogner, G.; and Mollwo, E.: Über Die Herstellung von Zinkoxygeinkristallen Mit Definierten Zusätzen. J. Phys. Chem. Solids, Vol. 6, 1958, pp. 136-143.

Delaney, R. A.; and Kaiser, H. D.: Polycrystalline Zinc Oxide Dielectrics. Abstract No. 16, IBM Systems Development Division, East Fishkill Facility, Hopewell Junction, N. Y., pp. 41-44.

Delaney, R. A.; and Kaiser, H. D.: Polycrystalline Zinc Oxide Dielectrics. J. Electrochem. Soc.: SOLID STATE SCIENCE, August 1967, pp. 833-842.

Dietz, R. E.; Kamimura, H.; Sturge, M. D.; and Yariv, A.: Electronic Structure of Copper Impurities in ZnO. Phys. Rev., Vol. 132, No. 4, November 15, 1963, pp. 1559-1569.

Ehrhardt, C. H.; and Lark-Horovitz, K.: Intensity Distribution in X-Ray and Electron Diffraction Patterns. Phys. Rev., Vol. 57, April 1, 1940, pp. 603-613.

Fehlner, Francis P.: Behavior of Ultrathin Zirconium Films upon Exposure to Oxygen. J. Appl. Phys., Vol. 38, No. 5, April 1967, pp. 2223-2231.

Fritzsche, Von O.: Elektrisches und optisches Verhalten von Halbleitern. X Elektrische Messungen an Zinkoxyd. Annalen der Physik, 5. Folge, Band 22, 1935, pp. 375-401.

Gerischer, H.: Electrochemical Behavior of Semiconductors under Illumination. J. Electrochem. Soc., Vol. 113, No. 11, November 1966, pp. 1174-1182.

Hartmann, W.: Elektrische Untersuchungen an oxydischen Halbleitern. Zeits of Physik, Vol. 102, 1936, pp. 709-733.

Infrared Studies of Nitrogenous Residues and Their Effects on Photocatalytic Properties of Zinc Oxide. N63-17980.

Jander, W.; and Stamm, Wilhelm: Der innere Aufbau fester anorganischer Verbindungen bei höheren Temperaturen. Zeitschrift für anorganische und allgemeine Chemie, Band 199, 1931, pp. 165-182.

Kohnke, E. E.: Optical and Electrical Properties of Stannic Oxide Crystals. AD 622 703, October 1965.

Lander, J. J.: Concentration of Hydrogen and Semiconductivity in ZnO under Hydrogen-Ion Bombardment. J. Phys. Chem. Solids, Vol. 3, 1957, pp. 87-94.

Levy, O.; and Steinberg, M.: The Adsorption of Carbon Monoxide on Zinc Oxide. Surface Science, Vol. 5, 1966, pp. 385-386.

Miller, P. H., Jr.: The Electrical Conductivity of Zinc Oxide. Phys. Rev., Vol. 60, December 15, 1941, pp. 890-895.

Mollwo, Von E.; and Stöckmann, F.: Über die elektrische Leitfähigkeit von Zinkoxyd. Ann. Physik [6], Vol. 3, p. 223, 1948.

Pourbaix, M. J. N.; and Rorive-Bouté, Madame C. M.: Graphical Study of Metallurgical Equilibria. Discussions Faraday Soc., Vol. 4, 1948, pp. 139-154.

Seiyama, Tetsuro; and Kagawa, Schuichi: Study on a Detector for Gaseous Components Using Semiconductive Thin Films. Anal. Chem., Vol. 38, No. 8, July 1966, pp. 1069-1070.

Stöckmann, F.: Über die elektrische Leitfähigkeit von Zinkoxyd. Z. Physik, Vol. 127, p. 563, 1950.

Van Hove, H.; Bohrmann, D.; and Luyckx, A.: Slow Ambient Insensitive Traps in Lithium Doped Zinc Oxide. Surface Science, Vol. 7, 1967, pp. 474-477.

Wagner, Carl: Theorie der georducten Mischphasen. Z. Physikal Ch. (B), Vol. 22, 1933, pp. 181-194.

"The aeronautical and space activities of the United States shall be conducted so as to contribute . . . to the expansion of human knowledge of phenomena in the atmosphere and space. The Administration shall provide for the widest practicable and appropriate dissemination of information concerning its activities and the results thereof."

—NATIONAL AERONAUTICS AND SPACE ACT OF 1958

NASA SCIENTIFIC AND TECHNICAL PUBLICATIONS

TECHNICAL REPORTS: Scientific and technical information considered important, complete, and a lasting contribution to existing knowledge.

TECHNICAL NOTES: Information less broad in scope but nevertheless of importance as a contribution to existing knowledge.

TECHNICAL MEMORANDUMS: Information receiving limited distribution because of preliminary data, security classification, or other reasons.

CONTRACTOR REPORTS: Scientific and technical information generated under a NASA contract or grant and considered an important contribution to existing knowledge.

TECHNICAL TRANSLATIONS: Information published in a foreign language considered to merit NASA distribution in English.

SPECIAL PUBLICATIONS: Information derived from or of value to NASA activities. Publications include conference proceedings, monographs, data compilations, handbooks, sourcebooks, and special bibliographies.

TECHNOLOGY UTILIZATION PUBLICATIONS: Information on technology used by NASA that may be of particular interest in commercial and other non-aerospace applications. Publications include Tech Briefs, Technology Utilization Reports and Notes, and Technology Surveys.

Details on the availability of these publications may be obtained from:

SCIENTIFIC AND TECHNICAL INFORMATION DIVISION

NATIONAL AERONAUTICS AND SPACE ADMINISTRATION

Washington, D.C. 20546